


## Review

# Critical Progress of Polymer Solar Cells with a Power Conversion Efficiency over 18%

Hongyue Tian <sup>1,†</sup>, Mingxin Zhao <sup>1,†</sup>, Xiaoling Ma <sup>1,\*</sup> , Chunyu Xu <sup>1</sup>, Wenjing Xu <sup>1</sup>, Zhongyuan Liu <sup>1</sup>, Miao Zhang <sup>2,\*</sup> and Fujun Zhang <sup>1,\*</sup>

<sup>1</sup> School of Physical Science and Engineering, Beijing Jiaotong University, Beijing 100044, China

<sup>2</sup> Department of Applied Biology and Chemical Technology and Research Institute for Smart Energy, The Hong Kong Polytechnic University, Hung Hom, Hong Kong, China

\* Correspondence: xlma2@bjtu.edu.cn (X.M.); bjtumiao.zhang@polyu.edu.hk (M.Z.); fjzhang@bjtu.edu.cn (F.Z.)

† These authors contributed equally to this work.

**Abstract:** The power conversion efficiencies (PCEs) of organic photovoltaics (OPVs) have reached more than 19%, along with the prosperous development of materials and device engineering. It is meaningful to make a comprehensive review of the research of OPVs for further performance improvement. In this review, some typical materials of high-performance OPVs are summarized, including representative polymer donor materials, non-fullerene acceptor materials, and interfacial modification materials, as well as their design rules for molecular engineering. From the point of view of device engineering, active layer treatment and deposition technology are introduced, which can play a critical role in adjusting the degree of molecular aggregation and vertical distribution. Meanwhile, a ternary strategy has been confirmed as an efficient method for improving the performance of OPVs, and the multiple roles of the appropriate third component in the photo-electronic conversion process are emphasized and analyzed. The challenges and perspectives concerning this region are also put forward for further developing high-performance OPVs.

**Keywords:** organic photovoltaics; ternary strategy; bulk-heterojunction; power conversion efficiency



**Citation:** Tian, H.; Zhao, M.; Ma, X.; Xu, C.; Xu, W.; Liu, Z.; Zhang, M.; Zhang, F. Critical Progress of Polymer Solar Cells with a Power Conversion Efficiency over 18%. *Energies* **2023**, *16*, 4494. <https://doi.org/10.3390/en16114494>

Academic Editor: Thanh-Tuân BUI

Received: 13 March 2023

Revised: 19 May 2023

Accepted: 31 May 2023

Published: 2 June 2023



**Copyright:** © 2023 by the authors. Licensee MDPI, Basel, Switzerland. This article is an open access article distributed under the terms and conditions of the Creative Commons Attribution (CC BY) license (<https://creativecommons.org/licenses/by/4.0/>).

## 1. Introduction

Organic materials have the advantage of solution processing, low cost, light weight, flexibility, easy fabrication, and abundant material resources [1]. Organic photovoltaics (OPVs) promises to be one of the major solar energy conversion technologies in our daily life. The bulk heterojunction (BHJ) type OPVs have stood out and made great progress in increasing the power conversion efficiencies (PCEs) in recent years [2]. The BHJ structure refers to a solution-processed active layer formed using the blend acceptor and donor solutions. Acceptor and donor materials interlace with each other, forming a bicontinuous interpenetrating network nanostructure [3]. Tang et al. invented a two-layer film configuration, in which the PCE of OPVs was only 0.95% in 1986 [4]. In 1995, Yu et al. first brought about the innovation of BHJ OPVs by using a fullerene acceptor and a conjugated polymer donor as active materials, which formed interpenetrating phase-separated D-A network morphology [5]. Fullerene-based OPVs produce relatively low PCEs because fullerene materials have some inevitable deficiencies, such as weak absorption in the visible-NIR region, morphological instability, and relatively fixed energy levels compared to non-fullerene materials [6]. Zhan et al. developed a novel acceptor, ITIC, by using a fused-ring core that was end-capped with INCN units in 2015 [7]. ITIC possesses good miscibility with polymer donors, good electron transport ability, broad and strong absorption, and appropriate energy levels. In 2019, Zou et al. developed Y6, composed of a central unit of a multi-fused ring and an electron-deficient benzothiadiazole core [8]. It achieved a certified PCE of 15.7% by being blended with polymer donor PM6 in the early days of its manufacture. Then, Y6 brought OPVs to a new level, and its derivatives became a research hotspot [9–18]. Many

high-performance donor materials have also been designed and synthesized, and the PCEs of OPVs have exceeded 18%. Figure 1 summarizes several representative works in the OPVs timeline.

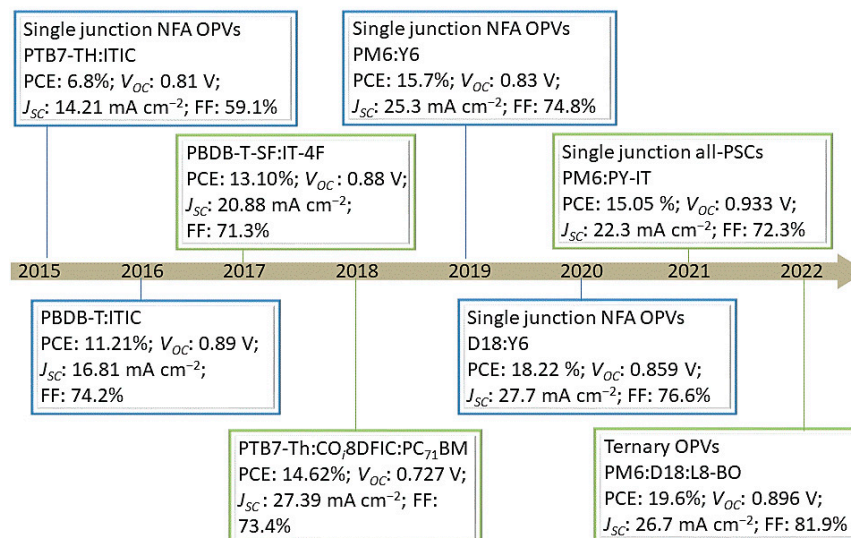


**Figure 1.** Timeline of the representative works in OPV research.

In this review, we summarize some representative functional layer materials with OPVs that have a high PCE. D18, PM6, and their derivatives were used as donor materials and have gradually become the leading donor materials. The acceptor materials have experienced a lot of innovations, including the synthesis of novel acceptor materials and the generation of new acceptors via chemical methods. Device engineering also plays a critical role in promoting the performance improvement of OPVs in addition to material innovations. The effects of additive engineering, the emerging layer-by-layer method, and the ternary strategy on the process of photo-electronic conversion are introduced in detail. Finally, the existing problems are emphasized, and the outlooks on the future investigation perspectives are offered to develop high-performance OPVs.

## 2. Working Mechanism of OPVs

The active layer is composed of a donor material and an acceptor material and is sandwiched between the hole and electron modification layer. The active layer of the BHJ structure is composed of a mixture of donor and acceptor materials. In an ideal BHJ, the two materials form a dual, continuous, and interpenetrating network with a large interface area and appropriate nanoscale phase separation, allowing for effective exciton separation and charge collection, respectively. OPVs have five basic physical processes (Figure 2) [19]:

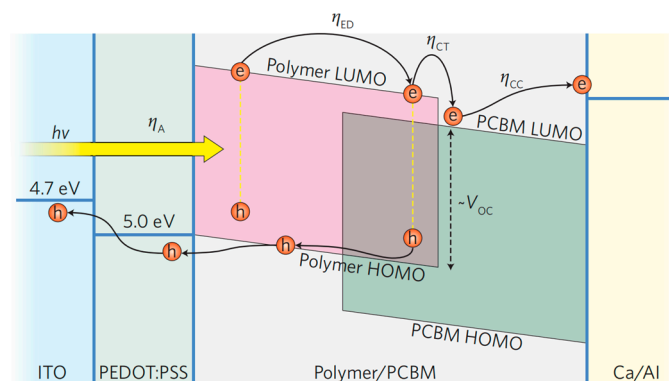


**Figure 2.** The operating mechanism of a polymer OPV. Reproduced from [19]. Reprinted with permission from ref. [19]. Copyright, 2012, Nature Photonics.

- (i) Photon absorption and exciton generation. In order to improve the light capture efficiency of OPVs, the BHJ active layer should have a wide absorption spectrum and a high molar extinction coefficient. The introduction of electron-absorbing groups or the addition of conjugated acceptor materials can effectively reduce the lowest unoccupied molecular orbital (LUMO) level and band gap and broaden the absorption spectrum, increasing the short circuit current ( $J_{SC}$ ) in total [20].
- (ii) Exciton diffusion to the donor-acceptor (D-A) interface. Excitons diffuse in the donor or acceptor phase, dissociate to free charge carriers at the D-A interface, or decay back to the ground state by radiative or nonradiative pathways after excitons are produced. The free charge needs to reach the D-A interface completely in order to improve the efficiency of exciton diffusion. Proper domain purity and size are necessary for improved exciton diffusion efficiency ( $\eta_{ED}$ ) and high  $J_{SC}$ . The blending film should have appropriate miscibility and crystallinity.
- (iii) Exciton dissociation. Excitons form charge transfer (CT) states at the D-A interface, which then completely dissociates into free electrons and holes. Excitons need to overcome the constraints of Coulomb forces. The difference in LUMO levels between the donor and acceptor effectively drives electron transfer. Regarding the mechanism of the D-A interface, the transition from the highest occupied molecular orbital (HOMO) level of the acceptor to the HOMO of the donor has been observed in non-fullerene acceptor (NFA)-based OPVs. The photons absorbed by the acceptor can also be used for photoelectric conversion, which helps increase the  $J_{SC}$  of the OPVs. Even if the difference in HOMO between the donor and acceptor is close to zero, the hole transfer is still effective. This helps to reduce the open circuit voltage ( $V_{OC}$ ) loss.
- (iv) Charge carrier transport. After the exciton dissociation, the free charge carriers will move toward their respective electrodes. The efficiency of free charge movement depends on the morphology of the film and the charge mobility characteristics of the semiconductor materials. The introduction of the D-A structure can realize inter-molecular charge transfer and increase the electron mobility of the acceptor material.  $J_{SC}$  and the fill factor (FF) were improved. The appropriate levels of distortion and alkyl chains can effectively influence morphology to enhance the  $J_{SC}$  and FF [20,21].
- (v) Charge carrier collection at individual electrodes. The holes and electrons arrive at the anode and cathode, respectively, forming an electric current. Charge collection efficiency ( $P_{coll}$ ) depends not only on the difference between the electrode and the D-A work function (WF), but also on the barrier at the organic compound/metal interface.

The efficiency of exciton diffusion depends on the size of the acceptor domain and the length of exciton diffusion. The size of the D-A domain is mainly determined by the morphology, while the diffusion length is controlled by the exciton lifetime (the coupling between the excited state and the ground state) and the relative probability of nonradiative decay. The charge transfer rate is determined by the coupling between the local excited state and the CT state, the energy shift between the local excited state and the CT state, and the recombination energy. The efficiency of CT exciton separation depends on the lifetime of the CT state, the coupling between the CT state and the charge separation (CS) state, the delocalization of electrons in the acceptor or holes in the donor, and the relative availability of the states.

The charge transport process is determined by the coupling between adjacent molecules, the degree of capture and desorption, and the lifetime of free charge carriers.  $P_{coll}$  depends on the degree of interface defects, the size of the extraction potential barriers, and surface velocity. These operational processes can be described as the competition between charge transfer (transport after the generation of free charges) and recombination after light absorption.

Singlet exciton migration and dissociation compete with the radiative and nonradiative decay to the ground state. Comparing the photoluminescence efficiency or exciton lifetime

of neat and blending materials is a common method to determine the exciton dissociation efficiency ( $\eta_{CT}$ ) [22].

$$\eta_{d,ex} = \frac{\tau_{neat} - \tau_{blend}}{\tau_{neat}}$$

The lowest excited singlet state for either the donor or acceptor requires excitons to reach the D-A interface within their lifetime to ensure charge transfer before excitons leave the interface or decay to the ground state. The efficiency of exciton diffusion to the interface is closely related to the multiphase morphology (size and purity of individual domains) of the BHJ blends. The energy difference between the lowest excited singlet state on either donor or acceptor and CT states [23] is represented as follows:

$$\Delta E_{CT} = E_{S1} - E_{CT1}$$

$\Delta E_{CT}$  is the driving force of exciton dissociation (charge transfer). The recombination and charge transfer rates can be determined by the molecular structures, orientation, and interactions, as well as the interactions with the environment of the donors and acceptors, which are still challenging.

This is involved in the four main parameters during the processes of carrier collection efficiency ( $\eta_{CC}$ ),  $\eta_{CT}$ , and  $\eta_{ED}$  and the absorption efficiency ( $\eta_A$ ). The external quantum efficiency (EQE) is a function of wavelength ( $\lambda$ ), which can also be expressed as [22]

$$EQE(\lambda) = \eta_{CC}(\lambda) \times \eta_{CT}(\lambda) \times \eta_{ED}(\lambda) \times \eta_A(\lambda).$$

$J_{SC}$  is the maximum current flowing through the device, originating from the internal field. The process of photon collection plays an important role in photocurrent. The donor and the acceptor are mixed to form the active layer to achieve photon absorption complementarity. The absorption of photons can be enhanced by increasing the thickness of the active layer, introducing a third component, and synthesizing new acceptor materials with strong near-infrared absorption and high extinction coefficients.  $J_{SC}$  is not solely reliant on the light collection ability of the active layer but rather is also influenced by exciton dissociation, charge transport, and the extraction processes that are microscopically determined.  $J_{SC}$  is influenced by all photovoltaic processes, in which (1) the production of excitons is heavily reliant on the absorption coefficient and the band gap of the donor; (2) the diffusion of excitons is influenced by the electronic structure, dielectric constant, and donor morphology (phase size) of the conjugated block; (3) exciton dissociation is influenced by the electronic structure, dielectric constant, and energy level shifts ( $\Delta E_{HOMO}$  and  $\Delta E_{LUMO}$ ) between the donor and acceptor; (4) the transport and collection of carriers are determined by the hole mobility of the donor and its balance with the electron mobility of the acceptor. High permittivity can decrease the exciton binding energy and recombination events. If the donor phase exceeds a certain size, the excitons that are generated in regions where the distance from the D-A interface is greater than the length of exciton diffusion will undergo recombination, leading to a reduction in  $J_{SC}$ .

In order to generate an external photocurrent, free charges must be extracted onto the electrode. This process is called diffusion or drift, which is represented by  $P_{coll}$ . Extraction does not compete with free-charge recombination in pairs but is also affected by traps and extraction barriers. One manifestation of this competition is the FF. Regardless of the exact mechanism of free-charge formation and recombination, the externally measured photocurrent density ( $J_{ph}$ ) is the result of at least four processes, each competing with a specific loss process. They can be expressed as the product of survival efficiency relative to each loss mechanism:

$$J_{ph}(F) = q\eta_{abs}\eta_{d,ex}\eta_{d,CT}(F)\eta_{coll}\phi_{inc}$$

in which  $\eta_{d,ex}$  and  $\eta_{d,CT}(F)$  refer to charge generation efficiency. Here,  $q$  refers to the charge,  $\phi_{inc}$  refers to the incident photon flux density, and  $\eta$  refers to the probability of the incident

photon being absorbed by the active layer.  $\eta_{d,CT}$  and  $\eta_{coll}$  depend on the internal electric field,  $F$ , and determine the shape of the density-voltage ( $J$ - $V$ ) property.

$V_{OC}$  originates from the splitting of the electron and hole quasi-Fermi levels:

$$V_{OC} = \frac{1}{e} (E_{Fn} - E_{Fp})$$

in which  $E_{Fp}$  and  $E_{Fn}$  refer to the hole and electron quasi-Fermi levels, respectively. The  $V_{OC}$  is determined by the difference between the  $E_{LUMO}$  of the acceptor and the  $E_{HOMO}$  of the donor, as well as by the dielectric constant of both the donor and acceptor. A lower  $E_{HOMO}$  of the donor can lead to a higher  $V_{OC}$ , while a larger dielectric constant can decrease the exciton binding energy and reduce the  $\Delta E_{LUMO}$  required for exciton dissociation, resulting in an increased  $V_{OC}$ . The  $V_{OC}$  is influenced by carrier density, light intensity and recombination, state density distribution, CT state, the microstructure of the blend, and the D-A interface area, which have limited impact on its determination.

The FF is determined by the competition between the recombination and extraction of free charge. It is defined as the ratio of the product of the  $V_{OC}$  and  $J_{SC}$  of the maximum power output ( $P_m$ ) of OPVs:

$$FF = \frac{P_m}{V_{OC} \times J_{SC}} = \frac{V_{mp} \times J_{mp}}{V_{OC} \times J_{SC}}$$

where  $V_{mp}$  and  $J_{mp}$  refer to the voltage and current density at the maximum power point, respectively. The value of the FF is affected by the charge transport process between the photoactive layers. The FF is greatly influenced by the hole mobility ( $\mu_h$ ) of the donor and the equilibrium with the electron mobility ( $\mu_e$ ) of the acceptor. The morphology of D-A blends also exerts a certain impact on the FF. Carrier mobility is affected by various factors, such as crystallinity and crystal orientation, side chains, building blocks, membrane morphology, and the number of structural defects. Structural defects refer to regional irregular units, terminal groups, a disordered arrangement of monomers in the copolymers, branches, light crosslinked units, etc. Most structural defects are challenging to identify, as they can have detrimental effects on crystallinity, morphology, and charge transport, ultimately leading to poor battery performance. The important composite mechanism in OPVs is the surface composition of the contact point, which is to extract the wrong type of carrier. The surface compound reduces the FF and increases the nonradiation composite loss of  $V_{OC}$ . The composition of the surface is created by the unintentional spread of the carrier to the wrong contact, and the harmful effect of this type of surface composition is the most prominent in the near-open road condition. The composition of the surface also affects the intensity dependence of  $V_{OC}$ . In order to improve contact and reduce the surface composition, the electrode's middle layer is usually used.

The main photovoltaic parameter PCE can be expressed as

$$PCE = \frac{J_{SC} \times V_{OC} \times FF}{P_{in}}$$

$P_{in}$  refers to the incident light power. The  $V_{OC}$  mainly depends on the HOMO and LUMO levels.  $J_{SC}$  is related to (i), (ii), (iii), (iv), and (v) mentioned above. The FF describes the “square” of the  $J$ - $V$  curve, which represents the “difficulty” of extracting the photo-generated carriers from OPVs. Each of the basic processes occurring in OPVs possibly becomes a bottleneck, limiting the efficiency of OPVs. For OPVs with high efficiency, the factors are summarized as follows: (i) photon harvesting capacity: the coincidence degree of the wavelength of sunlight range and the absorption photon range of the active layer, as well as the ability to generate excitons; (ii) the appropriate energy level arrangement and active layer morphology can realize efficient exciton dissociation and charge transport; (iii) the interfacial engineering of charge collection.



### 3. Materials Innovation

New materials are constantly being synthesized to improve the performance of OPVs. The synthesis of new active-layer materials needs to meet the following requirements: a wide absorption spectrum and strong absorption coefficient to capture as many photons as possible; appropriate energy levels to ensure a match with the donor or acceptor materials; good stability and excellent solubility, and so on. The interfacial modification layer is the intermediate layer connecting the active layer and the electrode. The selection and preparation of the interfacial modification layer strongly influence the charge transport and collection properties, which should also be considered when constructing efficient OPVs.

#### 3.1. Efficient Donor Materials

Low-bandgap (LBG), NFAs, and wide-bandgap (WBG) copolymer donor materials represent promising materials that have promoted PCEs to the 18% level in recent years. Creating more high-performance donor materials is another task to help realize more efficient OPVs. D18, PM6, and their derivatives have gradually become the leading donor materials thanks to their outstanding performance. The chemical constructions of efficient new donor materials are exhibited in Figure 3.

##### 3.1.1. D18, PM6, and Their Derivatives

Ding et al. first synthesized a novel D-A copolymer, donor D18, using DTBT, a fused ring acceptor unit, in 2019 [24]. The DTBT unit has the virtues of an extended molecular plane and strong electron-withdrawing capability, gifting D18 a deep HOMO level, strong  $\pi$ - $\pi$  stacking, and high hole mobility ( $1.59 \times 10^{-3} \text{ cm}^2 \text{ V}^{-1} \text{ s}^{-1}$ ). OPVs based on D18:Y6 reached a PCE of 18.22% (certified 17.6%). D18 and its derivatives have been the hot new materials for achieving efficient OPVs with a relatively high  $V_{OC}$ . D18 and other donor materials generally contain fluorine atoms, resulting in high synthesis costs. A cost-reduction strategy can be realized by replacing fluorine with chlorine. D18-Cl is a chlorinated analog of D18 with a deep HOMO level. When combining D18-Cl with NFA N3 as the active layers, the PCE of OPVs achieved a PCE of 18.13% (certified 17.6%) [25]. A side-chain strategy has been used to improve the photoelectric properties of materials and optimize the phase separation or molecular arrangement of active layers. In 2022, Yang et al. developed the hybrid side chains of the D18  $\pi$ -bridge and synthesized the polymers D18-C6Chp (hexyl-cycloheptyl), D18-C6Cp (hexyl-cyclopentyl), and D18-C6Ch (hexyl-cyclohexyl) [26]. A fresh type of hybrid side chain combines alkyl chains and rigid cyclics, which is different from traditional side chain modulation. The end cyclic chain with steric hindrance will interfere with the aggregation properties of polymers. It is hoped that the alkyl side chains allow for the compact packing of molecules. The D18-C6Chp, D18-C6Ch, and D18-C6Cp films have the ordered lamellar stacking distances of 20.2, 20.2, and 19.0 Å, separately, which are longer than those of D18 (17.8 Å). The average  $\pi$ - $\pi$  stacking distances of polymer D18-C6Ch and D18 were 3.58 Å and 3.54 Å. The crystallinity of the three polymers is similar to that of D18. Hybrid side chains can not only impact self-assembling features but can also facilitate interpenetrating network morphology when compared to simple branched or cyclic chains. Balanced charge transport, efficient exciton dissociation, and low charge recombination were endowed, resulting in a PCE of 18.20%, a  $V_{OC}$  of 0.91 V, and a FF of 78.7% [26]. PM6 and its derivatives have also been the new popular materials for achieving efficient OPVs. In 2015, Hou et al. explored PM6, a copolymer with BDD as the acceptor and BDT-F as the donor [27]. PM6 exhibits a HOMO level of  $-5.45 \text{ eV}$  and a bandgap of 1.80 eV. The low HOMO of PM6 is due to the introduction of two fluorine atoms on the BDT side chains. In 2018, Hou et al. developed PM7 by using a simple method of replacing critical fluorine with chlorine [28]. The morphological and optoelectronic properties of the two polymers are similar. The chlorinated polymer has a lower HOMO level than the fluorinated one, which is beneficial to increasing  $V_{OC}$ . The OPVs based on PM7:IT-4F achieved a PCE of 14.4%, which demonstrated the effectiveness of the chlorination.

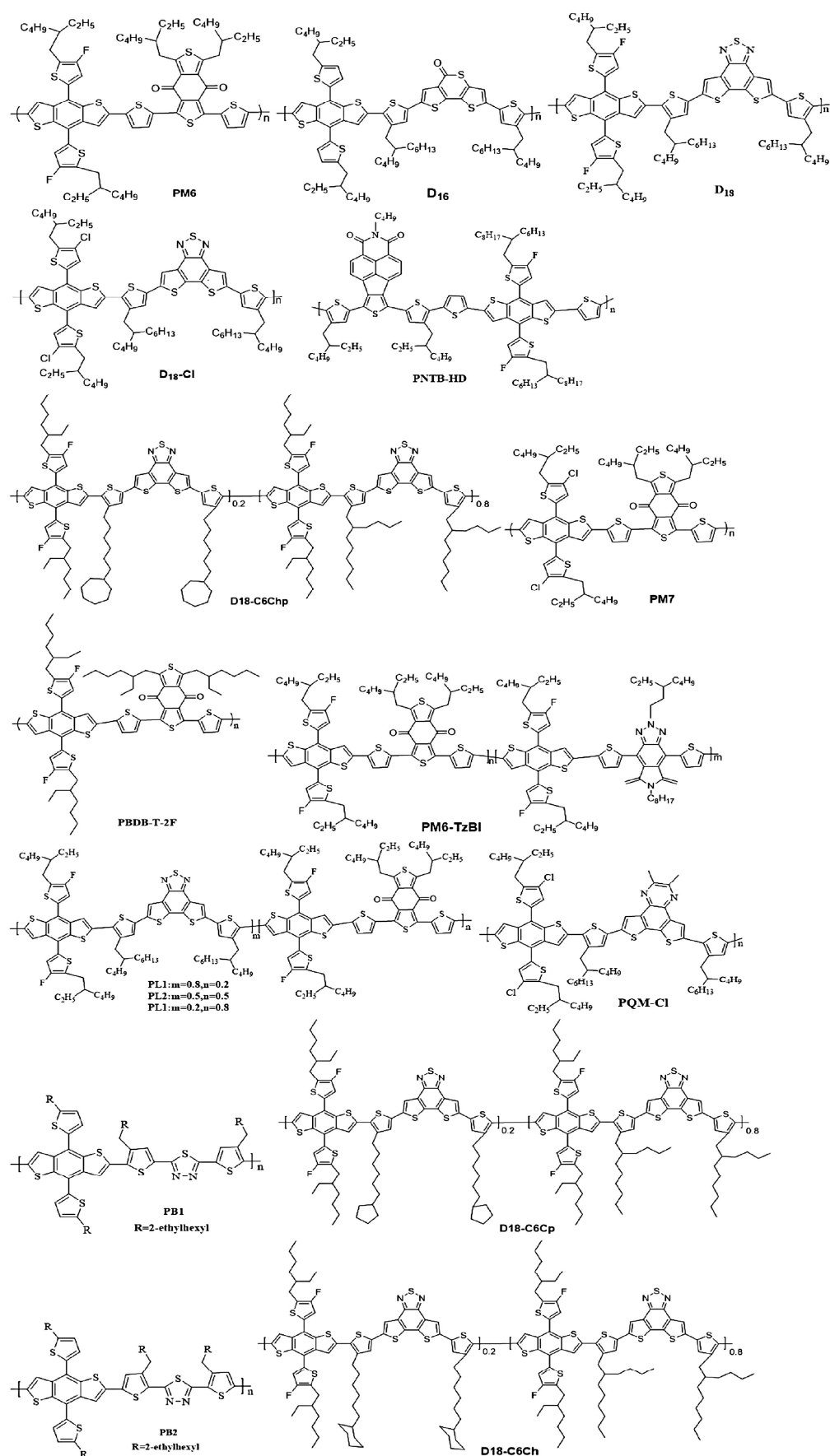


Figure 3. Representative chemical constructions of polymer donors.

### 3.1.2. Random Ternary Copolymerization Strategy

Random ternary copolymerization is a simple and powerful strategy to further develop and fine-tune those polymer donors with the best performance. A terpolymer is synthesized by introducing D<sub>2</sub> or A<sub>2</sub> units into the donor molecule or by replacing the units in the donor molecule. The performance of random copolymers depends to a large extent on the selection of the content of the added third unit and the compatibility with the skeleton. Peng et al. introduced a TzBI with high dipole and electron-deficient capabilities via the combination of A<sub>2</sub> units and the PM6 main chain and synthesized an efficient donor PM6-TzBI [29]. The D-A<sub>1</sub>-D-A<sub>2</sub> structure with TzBI unit tunes total electron deficiency. The dipole moment is introduced, which optimizes the morphology and has a low HOMO level. The OPVs based on PM6-TzBI-10:L8-BO showed a PCE of 18.36% by introducing 10% TzBI. Three polymer donors, PL3, PL2, and PL1 (ternary random copolymerization), were synthesized by Bo et al. by using repeat units of polymer donors D18 and PM6 [30]. The solubility and temperature-dependent aggregation behavior of PL1 in a halogen-free solvent improved when compared to PM6 and D18. The PL1:BTP-eC9-4F blends formed a uniform fibrous morphology with good phase separation, leading to an excellent PCE of 18.14%. Wang et al. developed a new random ternary polymer PM6-Si30 to replace the alkyl-substituted BDT units and 0.3 equivalent fluorine (F) in PM6 by introducing alkyl silica-substituted benzodithiophene (BDT) units and chlorine (Cl) as the third monomer [31]. The terpolymer PM6-Si30 has a relatively low HOMO level and slight blue shift absorption in comparison to PM6. It has good compatibility with PM6 and C9 and has good energetic properties because the terpolymer PM6-Si30 is similar to PM6 in structure. It can be used as the third component in the binary system. When PM6:C9 (D<sub>1</sub>:A) components were mixed with 15 wt% PM6-Si30 (D<sub>2</sub>), the PCE reached 18.27%,  $V_{OC}$  increased to 0.87 V,  $J_{SC}$  increased to 26.90 mA cm<sup>-2</sup>, and the FF increased to 78.04%. The enhanced performance of the PM6:PM6-Si30:C9-based ternary OPVs is mainly attributed to favorable phase separation, improved crystallinity, reduced recombination loss, and extended carrier lifetime in the active layer. Li et al. synthesized a new D-A<sub>1</sub>-D-A<sub>2</sub> type terpolymer PMT-CT-10, in which a 10% TTz A<sub>2</sub> unit is connected to the thiophene  $\pi$ -bridges, attaching the alkyl substituent toward the TTz A<sub>2</sub> units [32]. PMT-CT-10 has a good coplanar molecular structure and high absorption coefficient, as well as a high HOMO energy level. The blending membrane of PMT-CT-10 and acceptor Y6 have a good D-A interpenetrating network, which leads to enhanced surface orientation, an improved exciton ionization rate, and reduced charge recombination efficiency. The PCE of PMT-CT-10-based OPVs with Y6 as an acceptor reached 18.21%. Li et al. synthesized three terpolymers, named PMZ-30, PMZ-20, and PMZ-10, by adding PZ-T as an A<sub>2</sub> unit to the polymeric backbone of PM6 [33]. The HOMO levels of the three terpolymers gradually decreased, and the absorption coefficient was higher than PM6, resulting in corresponding OPVs with a relatively high  $V_{OC}$  and  $J_{SC}$  in comparison to the PM6-based OPVs. The PMZ-10:Y6-based OPVs reached a PCE of 18.23%. Lu et al. synthesized a series of new ternary polymers: OPz14, OPz13, OPz12, and OPz11, containing 50%, 20%, 10%, and 5% E-Tz, respectively, by using the skeleton of D18 and the readily available third component E-Tz [34]. All terpolymers exhibit deep HOMOs and are good when paired with Y6 to provide a high  $V_{OC}$  due to the electronegative properties of the E-Tz unit. The OPVs based on OPz11:Y6 achieved a PCE of 18.42% and a  $V_{OC}$  of 0.865 V.

### 3.1.3. Other Efficient Donors

There are also low-cost donor materials and ester-based donor materials that show great potential for application in addition to the donor materials of the D18 and PM6 series. Li et al. designed and synthesized a low-cost polymer donor poly (PTQ10), based on the D-A copolymerization concept, with difluorine-substituted quinoxaline as the acceptor unit and a simple thiophene ring as the donor unit [35]. PTQ10 has the advantages of a simple molecular structure, cheap raw material, two-step reaction, low synthesis costs, and an 87.4% total yield. PTQ10 has a wide strong absorption band in the wavelength



range of 450–620 nm, with a middle band gap of 1.92 eV and a low HOMO energy level of  $-5.54$  eV. With PTQ10 as the donor and a narrow-gap n-OS IDIC as the acceptor, the PCE of OPVs can reach up to 12.70%, and their photovoltaic properties are insensitive when the active layer thickness is between 100 nm and 300 nm, which is beneficial to the large-scale manufacturing of OPVs. Hou et al. designed and synthesized two BDT and dicarboxylic ester-substituted quaterthiophene-based polymers named PBDE4T-0F and PBDE4T-2F [36]. The molecular structure of PBDE4T-xF did not change much, but the fluorine substituents in PBDE4T-2F enhanced the interchain aggregation. The ester-modified polymer has a high tendency to aggregate in solution, which is conducive to reducing the aggregation size and  $\pi$ - $\pi$  packing distance of the blend film, achieving efficient exciton dissociation and symmetrical charge transport, which is caused by fluorine nonbonding interaction. Both polymers exhibit strong absorption in the 400–600 nm regions, which complements the absorption spectra of most high-performance A-D-A type small molecule acceptors (SMAs). PBDE4T-2F has a strong aggregation effect, which is conducive to significantly reducing the size of the polymer and forming a dense and ordered accumulation in the blend film. PBDE4T-2F:BTP-eC9-based blends have both highly efficient exciton dissociation and carrier transport, with a PCE of up to 16.1%. The morphologic difference can also cause the energy level shift of blends, which is the main factor in a change in voltage loss ( $V_{\text{loss}}$ ). Cao et al. developed a set of new PTs (P5TCN-Fx) by introducing the 3-cyanothiophene unit into the reference polymer P4T2F-HD and varied the backbone fluorination degree [37]. The HOMO of the new PTs is relatively high compared to that of P4T2F-HD in the range of 5.41–5.50 eV. Main-chain fluorination results in strong interchain interactions, improved polymer crystallinity, and appropriate miscibility (with Y6). Blends with P5TCN-F25 and P5TCN-F35 as electron donors form good morphologies with suitable phase separation and discontinuous interpenetration networks that contribute to efficient exciton dissociation, balanced charge transport, and inhibited recombination in OPVs. PCEs surpassing 16% have been achieved by both P5TCN-F25- and P5TCN-F35-based OPVs. In 2022, Hou et al. developed D-A polymer, PBQx-TCl, in which chlorinated benzodithiophene was connected to DTQx by using 2-butyloctyl-substituted thiophene units as bridges [38]. PQM-Cl was further synthesized by introducing two methyl groups into PBQx-TCl. The strong molecular aggregation was reduced, and solution-processability was improved in a green solvent because of the steric hindrance resulting from the introduction of the methyl groups. The PQM-Cl-based OPVs enabled a PCE of 18.0% due to balanced high-charge-carrier transport, favorable morphology, and low Urbach energy. Hou et al. developed two nonhalogenated conjugated polymer donors, PB2 and PB1 [39]. PB2 and PB1 have distinct thiophene side-chain orientations based on an aromatic skeleton, thiophene bridge, and BDT-TF. The PB2 and PB1 of thiophene-bearing alkyl chains have a TDz unit and a BDT unit separately. PB2 and PB1 share many similar photophysical and photochemical properties. PB2 has relatively strong aggregation in a solution in comparison to PB1 because it has a relatively good planar-conjugated backbone. PB1-based OPVs only reached a PCE of 5.3%; OPVs based on PB2 showed a good PCE of 17.7%. A PCE of 18.4% can be realized from ternary OPVs based on PB2:PBDB-TF:BTP-eC9, which is a good demonstration of the potential of PB2. Wu et al. synthesized donor PNTB-HD by decreasing the expansion of the alkyl chain of NTI, which can reduce steric hindrance around electronegative atoms [40]. Single crystal data showed that the intensity of short H-C and C=O interactions between adjacent molecules is affected by a reduction in bulkiness. PNTB-HD has a relatively strong tendency in chloroform solutions, relatively close packing in films, relatively high crystallinity, relatively good phase separation, favorable morphology in the mixture, and good hole mobility ( $8.07 \times 10^{-4} \text{ cm}^2 \text{ V}^{-1} \text{ S}^{-1}$ ) in comparison to those of PNTB-2T ( $6.48 \times 10^{-4} \text{ cm}^2 \text{ V}^{-1} \text{ S}^{-1}$ ) without treatment. PNTB-HD:N3-based OPVs have good thermal stability. PNTB-HD:N3-blended thin films show blurred fibrillar structures. The size of fibrillar structures for PNTB-2T:N3 is enlarged through continual thermal annealing at 65 °C for 128 h. It indicated that the blend of PNTB-HD:N3 has better morphology stability. The PNTB-HD-based OPVs showed a PCE of 18.15% by adding N3.

Efficient donor materials, such as D18, PM6, and their derivatives, as well as random ternary copolymerization polymers, have developed rapidly. In addition to improving the performance of OPVs based on donor material innovation, the demand for exploiting donor materials that are easy to synthesize, thermally stable, environmentally friendly, and have low costs is constantly increasing regarding future commercial production.

### 3.2. Efficient Acceptor Materials

The invention of new acceptor materials with the advantages of simple synthesis, energy level, band gap adjustment, and good morphology stability is quite imperative. The acceptors in OPVs have experienced a lot of innovations, including the synthesis of novel acceptors and chemical methods like side-chain modification, end modification, halogenation, and the transformation of different accepting and donating units during the past decade [41]. The chemical constructions of high-performance acceptors mentioned in this review are summarized in Figure 4.

#### 3.2.1. Small Molecule Acceptor

##### The Position and Length of Side Chains

Side-chain modification is a valid design strategy for optimizing photo-electronic properties, intermolecular interaction, charge transport, and aggregation morphology in thin films. Yan et al. invented new types of NFAs, BTP-4F-P3EH and BTP-4F-P2EH, by replacing the outer positions of BTP-4F-PC6 in different locations via branched alkyl chains [42]. BTP-4F-P2EH achieved reduced nonradiative recombination loss ( $\Delta E_{nr}$ ) and good blend morphology with PBDB-T-2F, achieving a PCE of 18.22%. The BTP-4F-P3EH-based OPVs reached a PCE of 17.57%, better than the BTP-4F-PC6-based OPVs (17.22%). In 2021, Sun et al. reported a sequence of NFAs L8-R (R is the alkyl chain) by introducing different aliphatic chains at various positions on the electronic construction of the Y6 backbone [43]. The structure of L8-BO with a 2-butyloctyl side chain is relatively ordered compared to Y6. L8-BO contributes to forming a bicontinuous interpenetrating network nanostructure with the donor. Balanced charge transport, low charge recombination, and high carrier generation can be achieved in L8-BO-based active layers. OPVs based on PM6:L8-BO showed a PCE of 18.32% (17.9% certified), with a FF of 81.5%,  $J_{SC}$  of 25.72 mA cm<sup>-2</sup>, and a  $V_{OC}$  of 0.874 V. Yang et al. developed a novel asymmetric SMA BTP-PhC6-C11 via exchanging the alkyl chains at the thiophene  $\beta$  position on Y6 to BTP-PhC6 [44]. The  $\eta_{CT}$  are 96.2% for PM1:BTP-PhC6-based OPVs, 97.1% for PM1:BTP-PhC6-C11-based OPVs, and 95.1% for PM1:Y6-based OPVs. OPVs based on BTP-PhC6-C11 have good exciton dissociation ability, which coincides with a high FF. The coherence length (CCL) of BTP-PhC6-C11 for both (001) and (100) peaks in the IP direction is relatively large compared to that of BTP-PhC6. The BTP-PhC6-C11 also displays a relatively large CCL and relatively small d-spacing compared with the Y6 from the GIWAXS picture for the (001) peak. The OPVs based on BTP-PhC6-C11 give strong molecular stacking and improved molecular crystallinity, which should be beneficial to charge transport. A PCE of 18.33% was gained for PM1:BTP-PhC6-C11-based OPVs. Except for Y6's derivatives, Huang et al. designed EH-HD-4F by using 2-hexyldecyl and 2-ethylhexyl side chains, substituting the alkyl chains on pyrrole for highly efficient OPVs with a PCE of 18.38% [45]. It can be seen that adjusting the NFA side-chain position is an efficacious tactic for adjusting the photovoltaic characteristics and molecular interactions of materials.

The length of the side chain is also a research hotspot except for the position of the side chain. In 2020, Hou et al. synthesized BTP-eC7 and BTP-eC9 by shortening the n-undecyl (C11) from n-heptyl (C7) to n-nonyl (C9) on the brink of BTP-4Cl-BO [46]. BTP-eC9, with relatively short alkyl chains, exhibits enhanced electron mobility, decreased Urbach energy, and suitable solubility in comparison to BTP-eC11. A maximum PCE of 17.8% for BTP-eC9-based OPVs can be achieved, along with  $J_{SC}$  = 26.2 mA cm<sup>-2</sup>, FF = 81.1%, and  $V_{OC}$  = 0.839 V. Wang et al. synthesized four acceptors, named BTP-4F-C5-16, BTP-4F-C6-16, BTP-4F-C7-16, and BTP-4F-C8-16, by extending the chain length from n-pentyl to n-octyl

on the bithiophene units in 2021, as shown in Figure 5a [47]. The molecular dihedral angles between the terminal units and central core can be varied from 7.9 to 16° with the change of alkyl chain length. BTP-4F-C5-16 has a relatively small dihedral angle, achieving relatively good molecular planarity for forming compact  $\pi$ - $\pi$  stacking. OPVs based on PM6:BTP-4F-C5-16 achieved a PCE of 18.20% with a FF of 77.68%,  $J_{SC}$  of 27.78 mA cm<sup>-2</sup>, and  $V_{OC}$  of 0.844 V, as shown in the Figure 5b. BTP-4F-C5-16 possessed the shortest alkyl chain, exhibiting good structural order, appropriate phase separation, and high electron mobility in its blend with PM6. BTP-4F-C5-16 has good planarity according to MDS measurement and DFT calculations, as exhibited in Figure 5c.

### Halogenation

In 2022, Chen et al. constructed an efficient A-D-A-type acceptor named CH17, featuring conjugated extension in the central and end directions, as well as fluorination [48]. The F atoms on the terminal unit are not different from Y6, which enhances the intermolecular interaction. The large conjugation extension and appropriate fluorination of CH17 afforded a strong 3D molecular network, reduced energetic disorders, improved charge transport, improved luminescence efficiency, upshifted CT state, much suppressed  $\Delta E_{nr}$ , and small energy loss ( $E_{loss}$ ) regarding the blend films. A PCE of 17.84% was reached in binary OPVs based on PM6:CH17, and a PCE of 18.13% was reached in ternary OPVs based on PM6:CH17:F-2F. Halogenations also focus on side chains or end units. Chen et al. designed and synthesized two NFAs (CH6 and CH4) with an A-D-A feature, which have identical backbones and characteristics of a  $\pi$  extension. The central molecular unit is converted from the phenazine conversion of Y6 by benzothiadiazole [49]. CH6 has additional fluorinations on the central unit, which has an impact on the molecular frontier. The LUMO and HOMO levels of CH6 are reduced in comparison to that of CH4, which favors the improvement of  $V_{OC}$  because of the high electronegativity of fluorine atoms. The CH6-based OPVs exhibit balanced mobility and high carrier transfer according to the space-charge limited current (SCLC) model. GIWAXS measurements showed that the PM6:CH6 blend has a relatively short  $\pi$ - $\pi$  packing distance of 3.63 Å in comparison to that of 3.76 Å for the PM6:CH4 blend. The enlarged CCL of 78.5 Å for the (100) diffraction peak in the IP direction and 24.5 Å for the (010) diffraction peak in the OOP direction can be reached for the PM6:CH6 blend when compared with that of 60.8 Å and 19.1 Å for the PM6:CH4 blend separately. The enlarged CCL suggested that PM6:CH6-based OPVs possess relatively good crystallinity, relatively ordered molecular packing, and an optimized morphology when compared with PM6:CH4-based OPVs. A PCE of 18.33% was reached for CH6-based OPVs, which is better than that of 16.42% for CH4 based-OPVs.

### Terminal Modification

Terminal modification is also used in molecular engineering, which conveniently operates and effectively improves OPV performance. Janjua designed a sequence of new all-small-molecule acceptors (ZMY1 to ZMY5) through the terminal modification of the ZR-Si4 molecule [50]. The PCEs and other parameters of fabricated OPVs were computed by time-dependent density functional theory, density functional theory, and other simulation calculations. The  $V_{OC}$  at a null voltage expressed better values than ZR-Si4. The designed molecules owned a better FF than ZR-Si4, with the ZMY1 molecule having the highest FF value. PCEs are estimated with certain parameters like  $V_{OC}$ ,  $J_{SC}$ , FF, and  $P_{in}$ , in which the PCE in the ZMY1 molecule is the highest value (PCE = 18.25%). Chen et al. decorated the BTP-eC9 molecule by adopting the CPTCN-Cl to replace IC-2Cl in the terminal unit and synthesized an asymmetric end-modified acceptor named AC9 [51]. The IC-2Cl unit could improve intermolecular interaction and intramolecular charge transfer, as well as reduce energy loss. The CPTCN-Cl unit could increase  $V_{OC}$  while ensuring a high  $J_{SC}$  and FF. The AC9 can utilize the advantages of the two terminal units. The appropriate bandgap polymer PM6 was selected as the donor based on the calculated LUMO and HOMO levels.

The PM6:AC9-based OPVs yielded a PCE of 18.43% (certified 18.1%), with an FF of 79%,  $V_{OC}$  of 0.871 V, and  $J_{SC}$  of 26.75 mA cm<sup>-2</sup>.

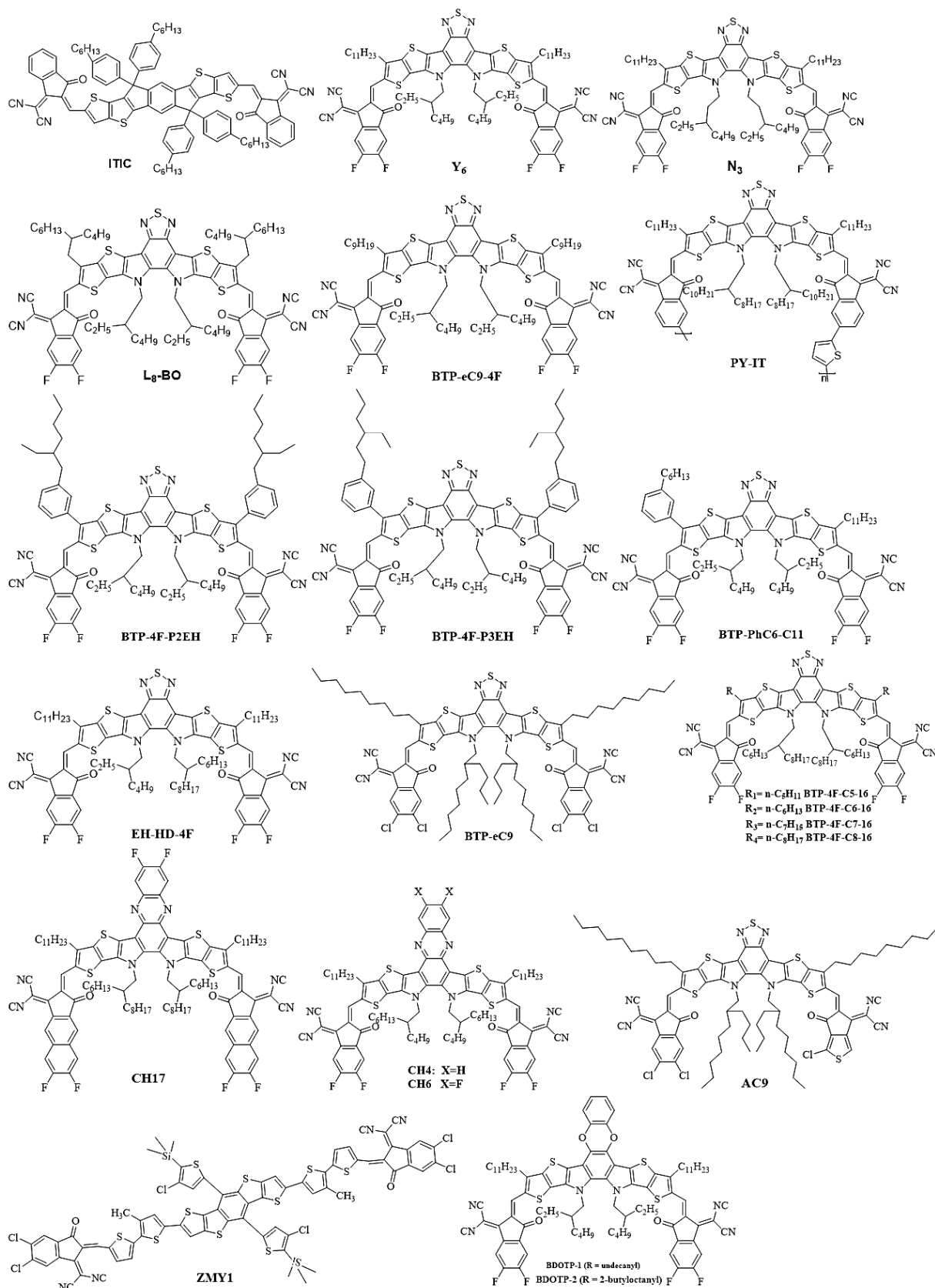
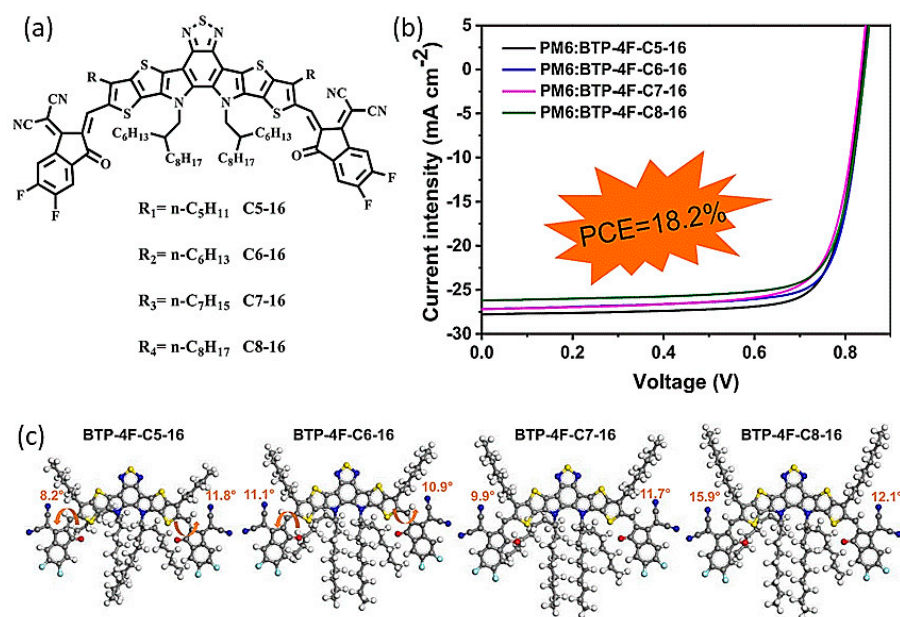


Figure 4. Representative chemical constructions of NFAs.



**Figure 5.** (a) Chemical constructions of BTP-4F-R-16 (R = C5, C6, C7, or C8). (b)  $J$ - $V$  curve. (c) Optimized geometries of four NFAs exhibiting different dihedral angles between the central core and terminal units. Reproduced from [47]. Reprinted with permission from ref. [47]. Copyright, 2021, American Chemical Society.

#### The Alternation of Electron-Accepting (A) and Electron-Donating (D) Segment

The change of electron-donating (D) and electron-accepting (A) units also represents a way to produce high-performance donor materials. In 2022, Ding et al. designed two acceptors similar to Y6, BDOTP-2, and BDOTP-1 [52]. An electron-rich dibenzodioxine fragment takes the place of an electron-deficient fragment within the core unit of BDOTP-2 and BDOTP-1, which leads to a significant change in the molecular dipole moment that is distinct from the former A-D-A'-D-A Y6-type acceptors. D18-B:BDOTP-2-based and D18-B:BDOTP-1-based OPVs exhibited a relatively high  $V_{OC}$  compared with D18-B:Y6-based OPVs. D18-B:Y6:BDOTP-1-based OPVs exhibited a relatively high  $V_{OC}$  in comparison to D18-B:Y6-based OPVs. The total  $E_{loss}$  was computed via the equation  $E_{loss} = E_{gap} - qV_{OC}$ . The  $E_{gap}$  values are 1.402, 1.402, 1.492, and 1.465 eV for D18-B:Y6:BDOTP-1, D18-B:Y6, D18-B:BDOTP-2, and D18-B:BDOTP-1, respectively. The high  $V_{OC}$  values of D18-B:BDOTP-2- and D18-B:BDOTP-1-based OPVs resulted from low  $\Delta E_3$  and large  $E_{gap}$ . The high  $V_{OC}$  of D18-B:Y6:BDOTP-1-based OPVs can be ascribed to the reduced  $\Delta E_3$ . The GIWAXS pattern presented a strong (100) lamellar stacking peak in the IP direction and a strong (010)  $\pi$ - $\pi$  stacking peak in the OOP direction in the D18-B:BDOTP-2 and D18-B:BDOTP-1 films. The D18-B:BDOTP-1 film had a large  $CCL_{010}$  and a short  $\pi$ - $\pi$  stacking d-spacing, benefiting the formation of a bicontinuous interpenetrating network and charge transport. PCEs of 18.51% and 16.93% have been reached in BDOTP-1-based ternary and binary OPVs, respectively. The high performance of Y6-type acceptors will predominantly depend on the banana-shaped structure rather than the A-D-A'-D-A configuration [52]. Table 1 describes the latest progress of OPVs with PCE values of more than 18%.

#### 3.2.2. Polymerized Small Molecule Acceptors

Inspired by the method of polymerizing small molecule acceptors, more and more novel polymer acceptors are emerging. The performance of polymerized small molecule acceptors (PSMAs) can be improved by controlling the reaction sites during polymerization, the direct regulation of skeleton-region regularization, end-group modification strategies, and the selection of appropriate additional linking units. PSMAs not only have the advantages of a non-fullerene small-molecule acceptor strong photon absorption ability in a specific region, as well as low energy loss and an adjustable energy level, but also have the



advantages of polymer material film-forming performance and optical and thermal stability. Duan et al. designed and synthesized two regio-regular nonfused PSMA, PFBTz-T- $\gamma$  and PFBTz-T- $\delta$ , by regulating the polymerization sites [53]. PFBTz-T- $\gamma$  has relatively dense and ordered packaging in the solid state, resulting in relatively great redshift optical absorption and relatively high electron mobility in comparison to PFBTz-T- $\delta$ . The PBDB-T:PFBTz-T- $\gamma$  blends exhibit efficient exciton dissociation, high and balanced charge transport, and less charge recombination. The absorption peaks ( $\lambda$ ) and the 0–0 and 0–1 absorption peaks of both polymers are located at nearly the same wavelength in solution. From solution to solid state, the 0–0 absorption peak of PFBTz-T- $\gamma$  is relatively strong and relatively weak compared with the 0–1 absorption peak of PFBTz-T- $\delta$ . This change shows that PFBTz-T- $\gamma$  is relatively ordered and has a relatively high absorption coefficient in comparison to PFBTz-T- $\delta$  in the solid state. The OPVs based on PBDB-T:PFBTz-T- $\gamma$  achieved a PCE of 9.72%, with a  $J_{SC}$  of 17.52 mA cm<sup>−2</sup> and an FF of 66%. Luo et al. developed three polymer acceptors: PY-IT, PY-OT, and PY-IOT [54]. The absorption edge of the three polymer acceptors gradually redshifted, the LUMO energy level gradually deepened, and the electron mobility monotonically increased. When the three polymers were blended with PM6, the PCEs of PY-IT-, PY-IOT-, and PY-OT-based OPVs reached 15.05%, 12.12%, and 10.04%, respectively. Wang et al. designed three narrow band gap acceptors, named PYTT-3, PYTT-2, and PYTT-1, using different isomers of thiophene-fused end-groups [55]. The effects of thiophene-isomerized terminal groups on the molecular structure, morphology, and physicochemical properties were studied. OPVs based on PyTT-2 exhibit relatively high PCEs when compared to the other two OPVs blended with PbDBT-T, which is mainly attributed to balanced charge transport, less charge recombination, and low nonradiation loss in the PyTT-2-based active layer. Yu et al. designed three types of PSMA, named PY-2T- $\gamma$ , PY-T- $\gamma$ , and PY-V- $\gamma$ , using dithiophene, thiophene, and ethylene as link agents, respectively [56]. The effects of different connection units on the physicochemical and photoelectric properties of PSMA were studied. PY-V- $\gamma$  molecules have good conjugation and tight interchain stacking properties, with high mobility and low energy disorder. The PCE,  $J_{SC}$ , and FF of PY-V- $\gamma$ -based OPVs were 17.1%, 24.8 mA cm<sup>−2</sup>, and 75.8%, respectively, after PM6 blending. The PCE of PY-T- $\gamma$  and Py-2t- $\gamma$ -based OPVs were 16.1% and 15.3%, respectively. The PY-V- $\gamma$ -based binary membrane has a high crystal ratio and a small amorphous phase length, which is efficient at transporting charge and inhibiting charge recombination in the active layer when compared to the other two blends. The research on polymer acceptors mainly focuses on PSMA. Various molecular optimization strategies were used to optimize the building units and connect the units and end groups of PSMA for realizing more idealistic morphological characteristics, photoelectric characteristics, and regional regularity.

The improved stability of OPVs plays a crucial role in the future development of commercialization in addition to improving the PCE of OPVs. Improving the intrinsic stability of molecules is the first step towards high stability OPVs. Examples include NFA chemical structure (e.g., heteroatomic substitution), energetics, structural rigidity, molecular conformation, and symmetry. PCE decay usually exists in OPVs using the BHJ structure due to the metastable morphology of the active layer. In the process of long-term aging, the active layer of a nano-channel with good phase separation will form too many scale aggregates, which is not conducive to the efficiency and life of the OPVs. OPVs performance using a BHJ structure is optimal when the active layer form is in a thermodynamic non-equilibrium state, which needs to be maintained throughout the thermal aging process. NFA structures customized to improve their thermal stability should not compromise PCE. Jen et al. developed a series of A-DA'D-A-type NFAs with varied side groups on the outward positions of the  $\pi$ -core, named BTP-H, BTP-Br, BTP-BO, BTP-TH, and BTP-TBr [57]. Acceptors with conjugated side groups exhibit good side group torsion and well-twisted backbones. They can provide up to 18.3% efficiency in xylene-processed cells. These acceptors with conjugated side groups have good thermal/optical stability. The



importance of NFA side-base steric hindrance to the stable balance of OPV performance should be emphasized.

The molecular design of NFAs plays a key role in driving the rapid efficiency gains of OPVs. The optical band gap, molecular structure, LUMO and HOMO energy levels, and structural characteristics (crystallization tendency) of NFAs can be effectively adjusted by molecular engineering. How to minimize the  $E_{\text{loss}}$  of OPVs based on molecular engineering should be one of the hot spots for future research directions.

### 3.3. Interfacial Modification Layer

Interface engineering is usually achieved by introducing an intermediate layer between the active layer and the electrode of OPVs, where the active layer is sandwiched between the anode and cathode. The development of the interlayer has been considered an important research area to achieve high OPVs performance and stability in addition to the design and synthesis of donor and acceptor materials. The modification layer is considered to be the key component for the preparation of OPVs. Liu et al. developed a new nonconjugated self-doped polymer zwitterion (s-PZ), which is the combination of polymer zwitterions and n-type doping effects [58]. Three s-PZs (NDI-M-DAN, PDI-N-DAN, and PDI-M-DAN) were synthesized using an uncomplicated scheme, which may discover better contact at the active layer interface based on the electrode/FREA, improving charge extraction and collection efficiency and reducing charge recombination loss. The PCE values of D18:Y6-based OPVs achieved a range from 17.60% to 18.17% by using the three s-PZs as the cathode interlayer (CIL). Zhang et al. synthesized three novel self-doped CIMs, named t-PyDINBr, t-PyDINO, and t-PyDIN, through the introduction of quaternary ammonium bromide, amino N-oxide, and amino as the functional groups [59]. The WF values changed from 4.50 eV (bare Ag) to 4.10 eV after applying an ultra-thin layer of spin-coated Ag electrodes. The t-PyDIN effectively reduced the Ag electrode WF, which is beneficial to forming ohmic contact at the organic semiconductor/metal interface and enhancing the internal electric field, improving the generation and collection of free charges. There are two independent molecular conformations in the crystal construction of t-PyDIN (Figure 6a) (named conformation A and conformation B). The  $\pi$ - $\pi$  stacking distance between the two molecules for conformation A and B is 3.445 Å and 3.491 Å, respectively. A larger  $\pi$ - $\pi$  stacking distance between conformation A and B of 3.491 Å occurs because of the steric hindrance of the tertiary amine side chains. The ordered intermolecular packing was surveyed (Figure 6b), as it is beneficial to charge transport. The t-PyDIN-based OPVs reached a PCE of 18.25%. The design and synthesis of high-performance small-molecule CIL have become the focus, which has good batch-to-batch reproducibility, a simple and clear molecular structure, and outstanding versatility. Sun et al. synthesized a conjugated small-molecule CIL called SME1 by applying a molecular tailoring tactic [60]. SME1 exhibits relatively low HOMO and LUMO levels when compared to the polymer counterpart. This advantage can improve blocking holes and extracting electrons. The ability to change the WF of the metal electrode and the inherent low surface energy of SME1 are beneficial to reducing the accumulation of space charge and optimizing the metal/molecule interfaces. The matched energy level arrangements enable SME1 to effectively collect electrons from both the NFA and polymer donor, resulting in improvements in charge collection and exciton dissociation. PM6:BTP-eC9-based OPVs achieved a PCE of 18.4% (17.9% through the third-party certification) by applying SME1 as CIL.

The development of hole transport layers (HTLs) is relatively backward compared to electron transport layers (ETLs). Most of the reported high-performance OPVs HTL basically choose the traditional OPV structure of polyethylenedioxythiophene:polystyrene sulfonate (PEDOT:PSS). PEDOT:PSS also has disadvantages, such as hygroscopicity and acidity, which can result in the severe chemical and physical degradation of OPVs from the point view of OPV stability. Since the organic molecules in the photoactive layer of OPVs inevitably come into contact with the intermediate layer, the contribution of interface stability to determining the lifetime of OPVs may become increasingly important.

Interlayers with ionic characteristics, such as PEDOT:PSS, can react chemically with NFAs, resulting in a decrease in the electronic performance of OPVs. The chemical reactivity is passivated by substituting less reactive ionic groups while maintaining charge selection. Peng et al. reported a Co-based HTL, which used the cost-effective Cobalt (II) acetate tetrahydrate ( $\text{Co}(\text{OAc})_2 \cdot 4\text{H}_2\text{O}$ ) as the precursor with simple processing [61]. TA and UVO treatments are performed to optimize the electronic properties of the Co-based HTL. The oxidized crystal water of the  $\text{Co}(\text{OAc})_2 \cdot 4\text{H}_2\text{O}$  precursor was reduced because of the TA process, improving the WF. The Co-based HTL suggested a low WF in comparison to the exposed ITO electrode (4.83 eV) after TA treatment. The resistance and morphology defects were reduced, and the conductivity and the WF improved with additional UVO treatment. A PCE of 18.77% was obtained by using OPVs based on PM6:L8-BO in Co-based HTL, with a high FF of 79.94%, a  $J_{\text{SC}}$  of  $26.37 \text{ mA cm}^{-2}$ , and a  $V_{\text{OC}}$  of 0.89 V, which is relatively high in comparison to PEDOT:PSS-based OPVs (18.02%).

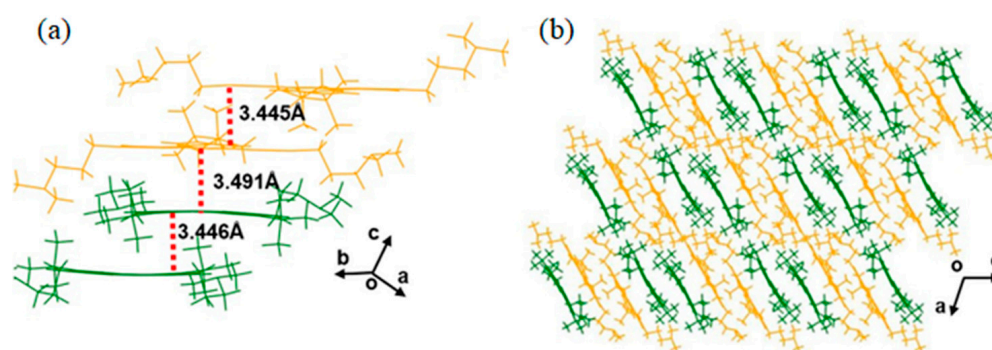


**Figure 6.** (a) The crystal  $\pi$ -stacking view of t-PyDIN (conformations A and B are marked as yellow and green, respectively) and molecular packing between the t-PyDIN molecules (b) along the  $\pi$ -plane. Reproduced from [59]. Reprinted with permission from ref. [59]. Copyright, 2022, Wiley.

Although the primary role of the mesosphere is to confer charge selectivity to OPVs, the chemical (or electrochemical) properties associated with the degradation caused by external sources (e.g., oxygen and water) and chemical interactions with NFAs are also important prerequisites for stabilizing OPVs. The modification layer also plays an important role in the stability of OPVs. More efforts should be devoted to improving the stability of OPVs by optimizing the interfacial modification layer. Meanwhile, the thickness of the current modification layer is usually very thin, which may not be suitable for future large-scale production technology. The synthesis of a novel interfacial modification layer with high stability and thickness-insensitive properties may be an important research direction for the commercialization of OPVs in the future.

**Table 1.** The recent progress of binary OPVs with an efficiency of over 18%.

Active Layer	$J_{\text{SC}}$ ( $\text{mA cm}^{-2}$ )	$V_{\text{OC}}$ (V)	FF (%)	PCE (%)	Year	Ref.
PQM-Cl:PY-IT	24.30	0.920	80.70	18.00	2022	[62]
PM6:Y6-BO	27.90	0.840	76.60	18.00	2021	[63]
D18-Cl:N3	27.85	0.859	75.70	18.13	2021	[25]
PL1:BTP-eC9-4F	27.11	0.876	76.41	18.14	2022	[30]
PNTB-HD:N3	26.88	0.854	79.00	18.15	2022	[40]
PM6:BTP-4F-C5-16	27.78	0.844	77.68	18.20	2021	[47]
D18-C6Ch:L8-Bo	25.46	0.910	78.70	18.20	2022	[26]
PBDB-T-2F:BTP-4F-P2EH	25.85	0.880	80.08	18.22	2021	[42]
D18:Y6	27.70	0.859	76.60	18.22	2020	[64]
PMZ-10:Y6	27.96	0.834	78.20	18.23	2022	[33]
PM6:L8-BO	25.71	0.870	81.50	18.23	2022	[65]
PM6:BTP-eC9	27.58	0.859	77.34	18.32	2022	[66]

Table 1. Cont.

Active Layer	$J_{sc}$ ( $\text{mA cm}^{-2}$ )	$V_{oc}$ (V)	FF (%)	PCE (%)	Year	Ref.
PM1:BTP-PhC6-C11	26.62	0.871	79.00	18.33	2022	[44]
PM6:CH6	26.62	0.875	78.40	18.33	2022	[49]
PM6-TzBI:L8-BO	25.63	0.897	79.84	18.36	2022	[29]
OPz11:Y6	27.02	0.865	78.71	18.42	2022	[34]
PM6:AC9	26.75	0.871	79.00	18.43	2022	[51]
PBDB-TF:BTP-eC9	26.60	0.866	80.30	18.50	2021	[67]
D18-B:Y6:BDOTP-1	27.74	0.859	77.60	18.51	2022	[52]
PM6:L8-BO-T2	26.73	0.889	79.32	18.85	2022	[68]

#### 4. Device Engineering

In addition to synthesizing new organic materials, device engineering should also play a vital role in improving the performance of OPVs, such as the additive addition strategy, layer-by-layer deposition strategy, and ternary strategy. Table 2 summarizes the latest developments in OPVs based on active-layer treatment and deposition techniques.

##### 4.1. Solvent and Solid Additive

Adjusting the morphology of the BHJ blend films is an important focus involving molecular orientation, crystallinity, and so on, which can affect exciton diffusion and dissociation, charge transport, and recombination [68]. Solvent additives are also commonly used in OPVs to regulate the molecular aggregation behavior during the evaporation process. Li et al. added 1-chloronaphthalene (CN) into a PBDBT:PYF-T chlorobenzene (CB) solution as a solvent additive [69]. The PCE reached 16.13%, and  $V_{oc}$  and FF increased to 0.86 V and 76.02%, respectively. The addition of the proper amount of CN can improve  $\pi$ - $\pi$  stacking in the PBDB-T:PYF-T system, which is conducive to charge transfer in the active layer to support the FF improvement of OPVs. The addition of appropriate CN can also reduce nonradiative recombination, which can help to improve the  $V_{oc}$  of OPVs. In addition to solvent additives, solid additives can also be used as a strategy to improve the performance of OPVs, which not only combine the advantages of solvent additives for adjusting molecular aggregation but also possess good volatilization properties for constructing more stable morphologies. Sun et al. introduced a solid additive named 1,4-diiodobenzene (DIB) to prepare highly efficient OPVs [70]. Adding DIB can optimize morphology and form a bicontinuous network to strengthen intermolecular packing in the donor and acceptor phases. The DIB contents affect the molecular packing of PM6. The fibril network morphology becomes obvious for the neat PM6 film treated with DIB as the DIB content increases to 300 wt%. The DIB makes the polymer donors self-assemble into clear fibril structures and induces Y6's aggregation. The fibril network morphology with proper phase separation was realized in a PM6:Y6 blend with 200 wt% DIB, which is in favor of charge transport and excitation dissociation. The crystallization and aggregation of PM6 (or Y6) improved because there is weak noncovalent interaction. Morphology is also controlled by DIB treatment by changing the concentration. The PM6:BTP-eC9-based OPVs produced a PCE of 18.13% (certified as 17.7%) with a FF of 79.8%. High  $V_{loss}$  also places restrictions on further improvements in OPVs, and it is important to develop effective approaches to reduce  $V_{loss}$ . Sun et al. reported OPVs based on NFA N3 and the polymer donor D18-Cl system by combining the sequential deposition (SD) method and DIB [71]. The D18-Cl/N3 (DIB) film shows increased crystallinity and adjustable phase separation by introducing DIB into N3. Angle-dependent GIWAXS measurements with the angle of incidence ranging from  $0.08^\circ$  to  $0.16^\circ$  were performed. The  $\pi$ - $\pi$  stacking  $CCL_{010}$  of acceptor and donor crystallites in the OOP direction was quantitatively evaluated by fitting the corresponding 1D profile (Figure 7a,b). The D18-Cl/N3 (DIB) blend film showed that the  $CCL_{010}$  value of the D18-Cl component along the vertical phase was significantly enhanced after DIB treatment. The self-assembly of N3 improved because of the DIB

additive. The charge transfer and extraction in D18-Cl/N3 (DIB) OPVs were enhanced due to the synergistic regulation of the acceptor/donor crystallinity in the whole vertical phase. The synergistic effects led to a PCE of 18.42% with an improved FF of 78.8% and a  $J_{SC}$  of 27.18 mA cm<sup>-2</sup> in OPVs based on D18-Cl/N3 (DIB). Sun et al. introduced an additive diiodomethane (DIM) into the PM6:L8-BO system [72]. Using DIM in place of 1,8-diiodooctane (DIO) reduced the energy difference between the charge transfer state in the PM6:L8-BO blend and the single excited state of L8-BO, resulting in a decrease in  $V_{loss}$  in OPVs. The OPVs with DIM treatment produced a PCE of 18.60% (certified as 18.20%) with an improved  $V_{OC}$  of 0.893 V. Zhang et al. designed two volatilizable SADs named SAD2 and SAD1 [68]. The planar SAD2 has the S...O noncovalent intramolecular interactions (NIIs). SAD1 is a distorted conformation. SAD2 has a relatively small space occupation when compared to SAD1, which can be more readily inserted between Y6 molecules, and this is conducive to the formation of a more compact Y6 intermolecular packing mode after thermal treatment. The OPVs with SAD2 treatment showed a high holes-transfer ratio, favorable morphology, balanced charge mobility, and less recombination loss. It is assumed that Y6-2, Y6-1, and Y6-0 refer to the Y6 film added by SAD2, the Y6 film added by SAD1, and the as-cast Y6 film, respectively. Y6-T2, Y6-T1, and Y6-T0 refer to the above Y6 films after corresponding follow-up TA treatment (140 °C, 100 °C, and 100 °C for 10 min, respectively). The absorption spectrum of the Y6-0 film consists of two main bands. One is the high absorption band at 300–420 nm, and the other is the low energy band at 420–920 nm with the maximum value of a  $\lambda$  ( $\lambda_{max}$ ) value at 834 nm. Those values of  $\lambda_{max}$  obviously are blue-shifted by 21 nm and 12 nm for Y6-2 and Y6-1, respectively, in comparison to the  $\lambda_{max}$  value of the Y6-0 film. Adding SADs disturbed the original intermolecular accumulation of Y6. The larger, blue-shifted value of Y6-2 showed that SAD2 may more seriously disrupt the  $\pi$ - $\pi$  stacking of Y6. The planar SAD2 is conducive to creating a relatively ordered intermolecular packing mode compared with SAD1 in the PM6:Y6 blend films. The effect of SAD conformation on the morphology of blend films was studied by 2D-GIWAXS. The  $CCL_{010}$  values of PM6:Y6-T2, PM6:Y6-T1, and PM6:Y6-T0 are 29.21, 28.29, and 25.31 Å, respectively. The SAD2-processed OPVs showed good morphology, balanced charge mobility, and less recombination loss, leading to a PCE of 18.85% (certified 18.7%) for the binary OPVs. Song et al. added the solid additive 2-methoxynaphthalene (2-MN) into the PM6:PY-DT system to regulate the molecular aggregation behavior during the film deposition and hot annealing process, which reached a PCE of 17.32% [73]. The working mechanism is that 2-MN induces the crystallization of PM6. The 2-MN gradually volatilizes and leaves room for the accumulation of PY-DT. The addition of 2-MN can obtain good active-layer morphology and ordered molecular stacking, realizing efficient charge collection and transport. Traditional active layer materials can also act as nonvolatile solid additives due to their special physicochemical properties. Li et al. added PC<sub>71</sub>BM as a solid additive to the PTzBI-oF:PFA1 blend [73]. Adding 1 wt% PC<sub>71</sub>BM can increase the PCE of OPVs from 14.6% to 15.6% while increasing  $J_{SC}$  and FF. Adding PC<sub>71</sub>BM that has a strong interaction with PTzBI-oF can reduce phase separation, weakening the charge recombination in the active layer. Additives engineering should be an effective method to adjust the molecular aggregation behavior of used materials for more efficient charge separation and transport in active layers.

#### 4.2. Layer by Layer

High-performance OPVs are mainly constructed using a BHJ structure, which enables the formation of interpenetrating networks with a large donor/acceptor interface area for effective exciton dissection. The photovoltaic performances of the blend casting (BC) OPVs are decided by a blending ratio of D:A, processing additives, and the conditions of the host solvents, etc. Sequential casting (SC), which is also called layer-by-layer treatment (LbL), can achieve analogous or even better OPV properties and morphologies when compared to BC processing. LbL OPVs and BC OPVs based on identical functional materials showed considerable performance, which suggests that the LbL method is an up-and-coming alter-



native for high PCEs in OPVs [9,74–79]. Chen et al. used the LbL program to manufacture OPVs [80]. The swelling intercalation phase separation (SIPS) model was proposed to explain BC and LbL processes (Figure 8a,b). The carrier dynamics were studied in OPVs in order to characterize the bias-dependent charge separation and collection behavior.  $\eta_{CT}$  in BC-type OPVs is 98.36% for PM6:L8-BO and 98.90% for LbL-type OPVs.  $P_{coll}$  is 89.09% for PM6:L8-BO systems and 90.56% for LbL-type OPVs. LbL-type OPVs showed obvious advantages in both  $\eta_{CT}$  and  $P_{coll}$  in comparison to BC-type OPVs, improving the FF of OPVs. The LbL-type OPVs exhibited slightly higher mobility than that of the BC-type OPVs, and the  $\mu_e/\mu_h$  value is 1.03. The LbL-type film has high exciton density and mobility balance in the middle, which is beneficial to increase OPV performance. The LbL method enabled PM6:L8-BO-based OPVs reach a PCE of 18.86% (18.44% certified). Zhang et al. constructed a series of OPVs with LbL and BHJ configurations using NFA Y6 and the polymer donor D18-Cl and introduced a dissociation-strengthening layer (DSL) to enhance the dissociation of D18-Cl excitons near ITO in LbL active layers [74]. The surface energy ( $\gamma$ ) values are 39.21, 38.31, and 44.33 mN m<sup>−1</sup> for DSL-modified D18-Cl-, D18-Cl-, Y6 films, respectively, which suggested existing interdiffusion between the DSL and the D18-Cl layer. The interface energy between Y6/D18-Cl and Y6 ( $\gamma_{Y6/D18-Cl:Y6}$ ) value (0.43 mN m<sup>−1</sup>) is relatively low compared with the  $\gamma_{D18-Cl:Y6}$  value (1.30 mN m<sup>−1</sup>). The reduced interface energy facilitated the diffusion of Y6 into the D18-Cl networks through the introduction of DSL, which enlarged the D/A interface to efficiently separate excitons in the LbL active layer. The LbL method enabled a PCE of 18.15% through the introduction of DSL, which benefited from an enhanced FF (75.79%) and  $J_{SC}$  (27.52 mA cm<sup>−2</sup>). Adding DSL provides a simple and efficient method for increasing the availability of exciton in LbL active layers.

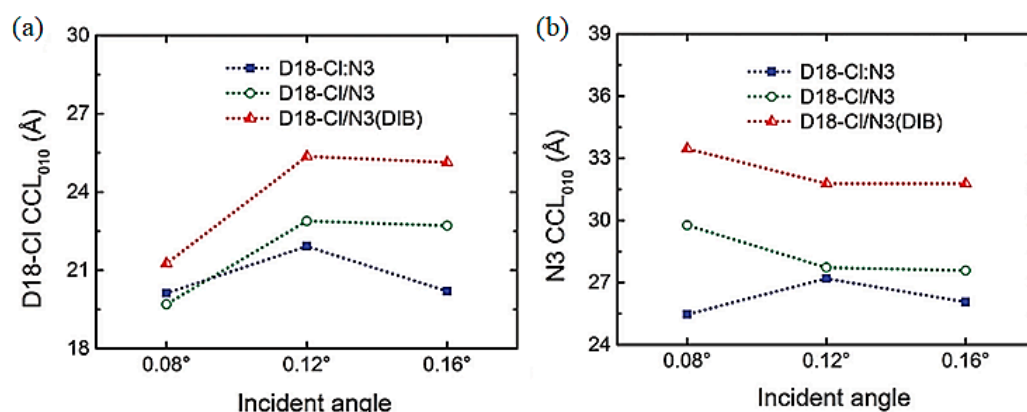


**Figure 7.** (a) D18-Cl and (b) N3 in three blend films at different incident angles. Reproduced from [71]. Copyright, 2022, Wiley.

Controlling the film morphology is difficult, particularly in the vertical D-A distribution. The SD sequence method involves the two-step deposition of the donor and acceptor materials. Huang et al. constructed binary SD OPVs based on L8-BO and D18 by SD, which is named SD<sub>2</sub> [81]. The SD<sub>2</sub> OPVs achieved a PCE of 19.05% (18.9% certified), which is relatively high compared with the BC OPVs (18.14%). The film-depth-dependent light absorption spectroscopy (FLAS) of the SD<sub>2</sub> film exhibited a red shift compared with the BC film, indicating that the crystallinity of the material in the SD<sub>2</sub> film is enhanced, which is conducive to charge transport. The composition distributions extracted from the FLAS supported good vertical phase separation in the SD<sub>2</sub> film (Figure 9a), in which acceptors and donors were rich on the surface and bottom of the active layer. The  $J_{ph}$  and the effective applied voltage ( $V_{eff}$ ) curves of the different OPVs were used to study the exciton dissociation and charge collection characteristics (Figure 9b). The values of  $J_{ph}/J_{sat}$  were 99.2% and 90.2%, respectively, and 98.2% and 89.1% for the SD<sub>2</sub> and BC OPVs, respectively, which suggested that the SD<sub>2</sub> showed more efficient charge collection and higher charge dissociation efficiency. Charge transport characteristics were studied through the SCLC region of

the pure electron OPVs and hole OPVs. Enhanced and balanced mobility ( $\mu_e/\mu_h = 1.06$ ) in SD<sub>2</sub> OPVs resulted in high FF values. The manipulation of vertical component distribution resulted in low energy loss, balanced charge transport, efficient exciton split, and high crystallinity in the films, which resulted in the all-around enhancement of  $J_{SC}$ ,  $V_{OC}$ , and FF. It is a simple and effective method to enhance photovoltaic performance by controlling the vertical component distribution of the active layer.

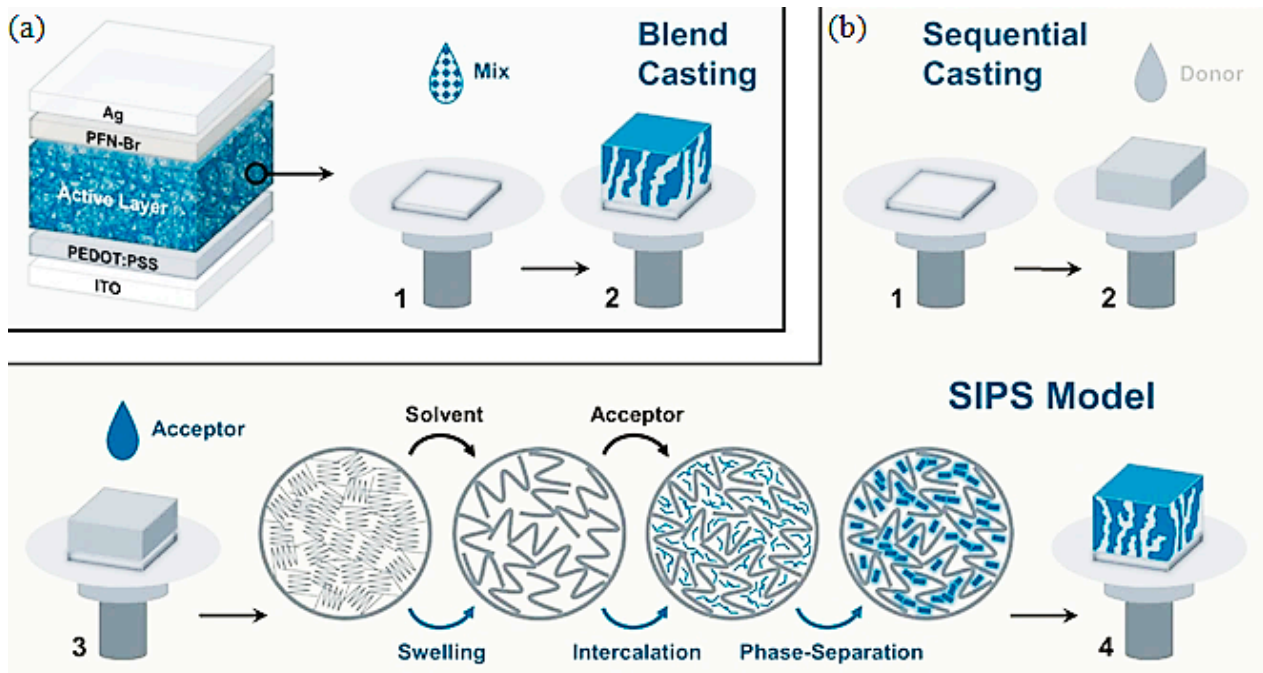


**Figure 8.** (a) Manufacturing procedure diagram of BC-type OPVs. 1. Deposition of donor and acceptor mixed solution; 2. Form a BHJ structure model. (b) Manufacturing process diagram of LbL OPVs and proposed SIPS model. 1. Deposition of PEDOT:PSS on the substrate; 2. Deposition of donor solution on PEDOT:PSS thin film; 3. Deposition of acceptor solution on PM6 thin films; 4. Form SIPS model. Reproduced from [80]. Reprinted with permission from ref. [80]. Copyright, 2022, Wiley.

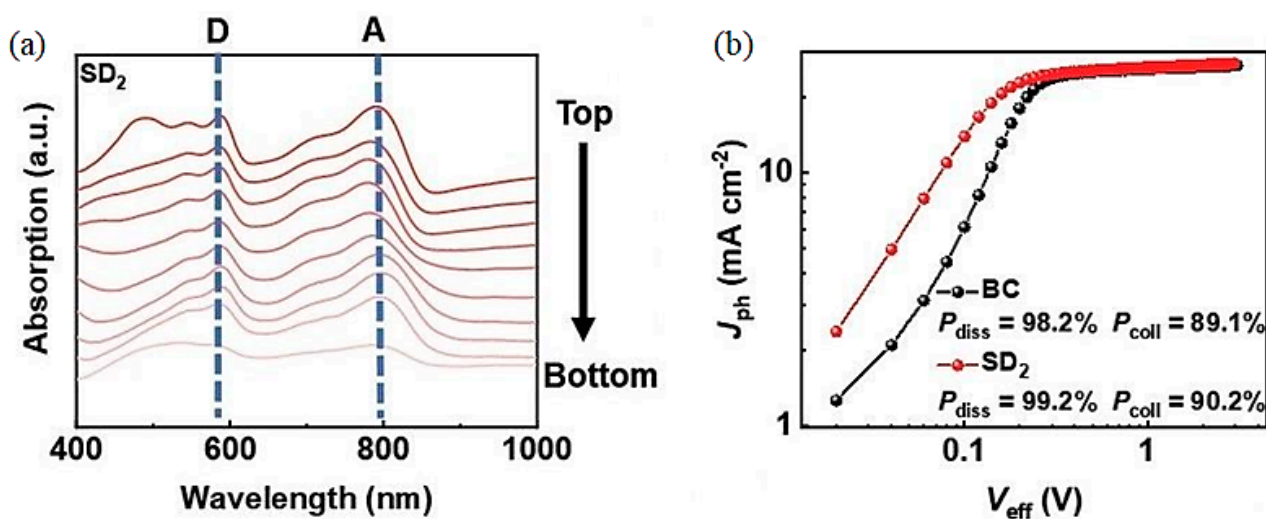


**Figure 9.** (a) SD<sub>2</sub> film (b)  $J_{ph}$ - $V_{eff}$ . Reproduced from [81]. Reprinted with permission from ref. [81]. Copyright, 2022, Wiley.



**Table 2.** Recent progress of OPVs based on active layer treatment and deposition technology with efficiency exceeding 18%.

Active Layer	$J_{sc}$ ( $\text{mA cm}^{-2}$ )	$V_{oc}$ (V)	FF (%)	PCE (%)	Year	Ref.
PM6:Y6--CS <sub>2</sub>	27.46	0.839	78.19	18.01	2022	[82]
PM6:BTP-eC9:PC <sub>71</sub> BM\2PACz	26.94	0.845	79.20	18.03	2020	[83]
PM6:BTP-eC9\HBC-S	26.51	0.860	79.22	18.05	2021	[84]
PM6:BTP-eC9 (DIB)	26.44	0.856	79.50	18.13	2022	[70]
D18:Y6\PDI-N-DAN	27.03	0.870	77.21	18.17	2022	[58]
PM6:BTP-eC9 (PVDF)	26.68	0.842	79.46	18.17	2022	[85]
D18:N3\NMA	27.23	0.864	77.30	18.20	2022	[86]
PM6:BTP-eC9:PC <sub>71</sub> BM\Cu003	26.70	0.856	79.70	18.20	2022	[87]
PM6:BTP-eC9\t-PyDIN	28.24	0.840	76.67	18.25	2022	[59]
PM6:BTP-eC9:PC <sub>71</sub> BM (DQ)	26.93	0.856	79.40	18.30	2020	[87]
PM6:Y6 (DMBI-BDZC)	26.79	0.853	80.20	18.33	2022	[88]
PM6:BTP-eC9\SME1	27.60	0.852	78.30	18.40	2022	[60]
PM6:BTP-eC9:PC <sub>71</sub> BM\Br-2PACz	27.10	0.864	78.60	18.40	2021	[89]
D18-Cl/N3 (DIB)	27.18	0.860	78.80	18.42	2022	[71]
PM6:PM7-Si:BTP-eC9 (BV)\Cl-2PACz	26.96	0.863	79.40	18.50	2022	[90]
PM6:PBB1-F:BTP-eC9 (PAE)	27.44	0.859	78.51	18.51	2022	[91]
PM6:BTP-eC9:PC <sub>71</sub> BM\MPFM	28.00	0.847	78.14	18.53	2022	[92]
PM6:L8-BO (DIM)	26.03	0.893	26.03	18.60	2021	[72]
PM6:L8-BO\Co-based	26.37	0.890	79.94	18.77	2021	[61]
PM6:L8-BO--SC	26.61	0.883	80.39	18.86	2022	[80]
D18:L8-BO--SD <sub>2</sub>	26.86	0.918	77.25	19.05	2022	[81]
PTQ10:BTP-FTh:IDIC (DTT)	27.17	0.870	80.60	19.05	2022	[93]

( ) stands for additive; \ stands for modification layer; -- stands for preparation method.

#### 4.3. Ternary Strategy

The photon harvesting of the traditional binary active layer is usually limited due to the relatively narrow absorption spectra of organic semiconductor materials. Introducing the third component as a donor or acceptor can enhance the ability of the active layer to capture photons, increase the value of  $J_{sc}$ , and enable OPVs to achieve high PCE. The OPV parameters for some high-performance ternary OPVs are summarized in Table 3. According to the function of the third component, ternary OPVs can be divided into two donors/one acceptor and one donor/two acceptors. The ternary strategy has attracted widespread attention. It not only maintains the simple process of single-layer OPVs but also expands the photon capture capability of the active layer. In addition to enhancing photon capture ability, the performance of OPVs can also be improved by adjusting the energy level, reducing energy loss, and optimizing morphology. The dynamic process in ternary OPVs mainly depends on the function of the third component. The third component could (i) locate at the donor/acceptor interface, (ii) form its own channels, (iii) be fully embedded in one particular host domain, or (iv) form an alloy with the acceptor or donor materials. The location of the third component in the active layer is closely related to basic principles in ternary OPVs. Ternary OPVs have four working mechanisms: alloy model, parallel linkage, energy transfer, and charge transfer [94–97]. The four working mechanisms explain the interaction between the third component and the main system. The complementary absorption of the host binary system and the third component are usually considered to improve the photon harvesting ability of the active layers. In addition to absorption spectra, the energy levels also need to be taken into account to prevent the formation of deep charge traps in the ternary active layers. The addition of relatively low/high HOMO/LUMO levels of donor or acceptor can promote the improvement of the  $V_{oc}$  of ternary OPVs when compared with the principal binary system. At the same time, compatibility between the materials is the key factor that determines the degree of separation and dynamic process

of the active layer. The absorption spectra, energy level, and compatibility properties are usually considered when selecting the third component.

**Table 3.** Recent progress of ternary OPVs with efficiency over 18%.

Active Layer	$J_{SC}$ (mA cm <sup>-2</sup> )	$V_{OC}$ (V)	FF (%)	PCE (%)	Year	Ref.
PM6:Y6:AQx-3	26.82	0.870	77.20	18.01	2021	[98]
PM6:BO-4Cl:BTP-S2	27.11	0.856	77.98	18.03	2022	[99]
PM6:m-BTP-PhC6:Y6	26.28	0.870	78.21	18.05	2022	[100]
PM6:TTBT-R:Y6	27.01	0.862	76.13	18.07	2022	[101]
L4:N3:PC <sub>61</sub> BM	27.07	0.850	78.70	18.10	2022	[102]
PM6:Y7-BO:Y6-1O	26.35	0.867	79.27	18.11	2022	[103]
PM6:m-BTP-PhC6:Y6	26.53	0.870	78.51	18.12	2022	[100]
Z2:PM6:BTP-eC9	27.22	0.855	77.84	18.12	2022	[104]
PM6:ITIC-M:Y6	26.36	0.859	80.10	18.13	2022	[105]
PM6:CH17:F-2F	26.62	0.889	76.60	18.13	2022	[48]
PM6:PBB1-F:BTP-eC9	26.94	0.861	78.28	18.16	2022	[27]
PM6:BO-4Cl:BTP-S2	27.14	0.861	78.04	18.16	2022	[99]
PM6:Y6:PC <sub>71</sub> BM	27.92	0.846	77.13	18.21	2022	[92]
PM6:BTP-eC9:PC <sub>71</sub> BM	27.64	0.852	77.53	18.25	2022	[92]
PM6:PM6-Si30:C9	26.90	0.870	78.04	18.27	2022	[31]
PM6:BTP-BO-4F:BTA2	26.76	0.869	78.55	18.27	2022	[106]
PM6:BTP-eC11:BTP-S2	26.62	0.872	79.00	18.31	2022	[107]
PTQ10:BTP-FTh:IDIC	26.97	0.867	78.60	18.39	2022	[93]
PB2:PBDB-TF:BTP-eC9	26.90	0.858	79.70	18.40	2022	[39]
PM6:BTP-eC9:BTP-F	26.99	0.858	79.70	18.45	2021	[108]
PM6:BTID-2F:L8-BO	26.86	0.889	77.52	18.52	2022	[109]
PM6:Y6-1O:BO-4Cl	27.46	0.855	79.00	18.52	2022	[110]
PBDB-TF:PB2F:BTP-eC9	26.80	0.863	80.40	18.60	2021	[111]
D18:reg-PThE-1F:L8-BO	26.39	0.921	76.71	18.64	2022	[112]
PM6:L8-BO:eC9-2Cl	26.63	0.89	78.74	18.66	2022	[13]
PM6:BTP-eC9:L8-BO-F	27.35	0.853	80.00	18.66	2021	[113]
PBDB-TF:BTP-eC9:BTP-S2	26.78	0.878	79.44	18.66	2022	[114]
D18-Cl:N3:PC <sub>61</sub> BM	28.22	0.849	78.00	18.69	2021	[115]
PM6:BTP-eC9:ZY-4Cl	27.40	0.863	79.00	18.69	2022	[116]
PM6:BTP-eC9:AITC	27.20	0.870	79.70	18.80	2022	[117]
PBDB-TF:HDO-4Cl:eC9	27.05	0.866	80.51	18.86	2021	[118]
PM6:BTP-H2:L8-BO	26.68	0.892	80.70	19.02	2022	[119]
PM1:L8-BO:BTP-2F2Cl	27.15	0.881	80.14	19.17	2022	[120]
PM6:L8-BO:BTP-S10	26.80	0.898	80.22	19.26	2022	[121]
PM6:D18:L8-BO	26.70	0.896	81.90	19.60	2022	[122]

#### 4.3.1. Enhanced Photon Harvesting

The narrow absorption range of organic semiconductors leads to insufficient photon capture, resulting in low values for  $J_{SC}$ . When compared to binary blends, the introduction of a third component achieves a relatively wide absorption range, increases the value of  $J_{SC}$ , and achieves relatively high PCE for ternary OPVs.  $J_{SC}$  is usually proportional to photon capture in the active layer. The use of two tunable bandgap NFAs as two acceptors for ternary OPVs can broaden the photon absorption range of the active layer, increasing the value of  $J_{SC}$  and improving OPV performance. Zhang et al. reported ternary OPVs through the introduction of an L8-BO-F acceptor to the PM6:BTP-eC9 blend [113]. L8-BO-F shows a very similar chemical constitution to BTP-eC9, with a different side-chain length and the same molecular backbone. The UV-vis absorption profiles of the blend and neat films are shown in Figure 10a,b. The absorption of L8-BO-F is completely complementary to that of BTP-eC9 and PM6. Adding L8-BO-F to the PM6:BTP-eC9 blend improves the absorbance coefficient of the ternary blend, which is conducive to improving the photocurrent and increasing the amount of light harvesting. The  $J_{SC}$  increased to 27.35 mA cm<sup>-2</sup>, the  $V_{OC}$  increased to 0.853 V, and the FF increased to 80.0%. The high  $J_{SC}$  is mainly attributed to the

complementary absorption of L8-BO-F, BTP-eC9, and PM6. The extracted  $\alpha$  values are 0.99, 0.95, and 0.97 for the ternary, PM6:L8-BO-F, and PM6:BTP-eC9 OPVs, respectively, which showed that the biomolecular recombination is very weak in the ternary OPVs (Figure 10c). The slopes of the PM6:BTP-eC9:L8-BO-F, PM6:L8-BO-F, and PM6:BTP-eC9 OPVs are 1.05, 1.26, and 1.10 kT/q, respectively. The PCE of the ternary OPVs reached 18.66% after adding 15 wt% L8-BO-F. Zhao et al. developed an asymmetric small molecular donor TTBT-R [101]. The ternary OPVs based on PM6:TTBT-R:Y6 obtained a PCE of 18.07% with 10 wt% TTBT-R. PM6 and Y6 showed strong absorption in 600–900 and 500–650 nm bands, respectively. TTBT-R was introduced into the PM6:Y6 host system as a guest donor to strengthen light harvesting in the active layer at 445–560 nm, which is beneficial to improving the  $J_{SC}$  values. This largely resulted in an increase in  $J_{SC}$  from 26.45 to 27.01 mA cm<sup>-2</sup>, with the broad light harvesting of TTBT-R. The melting points of TTBT-R in the TTBT-R:Y6 and TTBT-R:PM6 blends reduced to 172.4 °C and 167.8 °C, respectively. The crystallization points of TTBT-R in the TTBT-R:Y6 and TTBT-R:PM6 blends reduced to 119.3 °C ( $\Delta H = 1.6$  J g<sup>-1</sup>) and 114.9 °C ( $\Delta H = 1.2$  J g<sup>-1</sup>), respectively. It is noticed that TTBT-R has relatively good compatibility with PM6 in comparison to Y6. TTBT-R is easily dispersed when in the donor phase in ternary blends, resulting in less charge recombination and efficient exciton dissociation. The ternary OPVs showed that  $V_{OC}$  increased to 0.885 V with increasing TTBT-R weight.

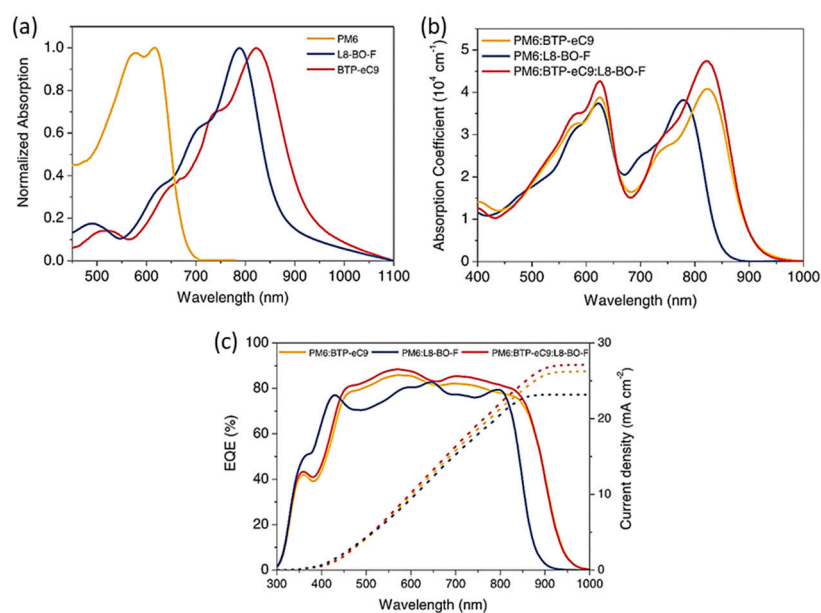


**Figure 10.** (a) UV-vis spectra of PM6, BTP-eC9, and L8-BO-F films. (b) UV-vis spectra of the binary and ternary blends. (c) EQE spectra (solid lines) and the integrated  $J_{SC}$  (dashed lines) of the binary and ternary OPVs; reproduced from [113]. Reprinted with permission from ref. [113]. Copyright, 2022, Royal Society of Chemistry.

#### 4.3.2. Adjusting Energy Levels

The energy shift between the donor HOMO and acceptor LUMO levels is crucial for successful charge dissociation and exciton splitting in OPVs. The  $V_{OC}$  of OPVs is proportional to the difference in energy levels between the donor HOMO and acceptor LUMO. The charge and energy transfer characteristics of the donor and acceptor interface can be altered by adjusting the HOMO-LUMO gap between the donor and acceptor. The ternary method is a simple preparation process that introduces an additional third component into the main binary system, which can achieve the fine-tuning of the energy level position of an alloyed state. Lin et al. developed a random terpolymer named PM6-Si30 that was introduced into PM6:C9-based OPVs as a guest donor [31]. PM6-Si30 shows a slightly blue-shifted absorption and relatively low HOMO level in comparison with PM6. The structure of PM6-Si30 is similar to PM6 and has good miscibility with both the PM6 and

C9. The LUMO/HOMO levels are  $-3.20/-5.45$  eV and  $-3.19/-5.56$  eV for PM6 and PM6-Si30, respectively (Figure 11a). The optimal blend based on PM6:PM6-Si30 exhibited the analogous LUMO and HOMO energies, which can form alloys. The expected slope of the bimolecular recombination-dominated OPVs in the natural logarithm diagram of  $V_{OC}$  and light intensity is  $1\text{ kT}/q$ , where  $k$  refers to the Boltzmann constant,  $q$  refers to the elementary charge, and  $T$  refers to temperature. The PM6:C9-based OPVs exhibited a slope of  $1.12\text{ kT}/q$ , which showed that there is recombination because of the traps. The trap-assisted recombination decreased (slope  $1.04\text{ kT}/q$ ) when 15 wt% PM6-Si30 was added (Figure 11b). The ternary OPVs based on PM6:PM6-Si30:C9 resulted in a PCE of 18.27% with the optimal ratio. Chen et al. developed a new NFA named BTP-H2, which has relatively strong crystallinity and up-shifted energy levels in comparison to the L8-BO molecule [119]. The matching of BTP-H2 and the polymer donor PM6 is conducive to effective charge separation. The BTP-H2 film has a relatively steep absorption edge in comparison to the L8-BO film, which suggested that the molecular stacking in a solid state is more orderly. Both the HOMO and LUMO of BTP-H2 are mildly high in comparison to that of L8-BO. The HOMO shift ( $\text{HOMO}_{\text{PM6}} - \text{HOMO}_{\text{NFA}}$ ) between BTP-H2 and PM6 is reduced to 40 m eV. An effective way to reduce  $\Delta E_{\text{nr}}$  is to narrow the HOMO shift between the donor and acceptor (even close to zero). The  $\alpha$  values of  $P_{\text{light}}$  (PM6:L8-BO:BTP-H2 and PM6:BTP-H2 are both 1.00; PM6:L8-BO is 0.97) show that BTP-H2 is favorable for charge extraction. The BTP-H2 can improve the charge extraction and inhibit trap-mediated single-molecule charge recombination, which is helpful for  $V_{OC}$  and  $J_{SC}$  in ternary OPVs. EQE<sub>ET</sub> and Fourier transform photocurrent spectroscopy external quantum efficiency (FTPS-EQE) experiments were used to analyze energy loss. The PM6:BTP-H2-based OPVs deliver the minimum whole  $E_{\text{loss}}$  (0.534 eV) among the three OPVs. The ternary OPVs appear to have relatively low  $E_{\text{loss}}$  (0.563 eV vs. 0.558 eV) compared to the control OPVs based on PM6:L8-BO. Introducing BTP-H2 helps to inhibit the nonradiative decay of controlled OPVs. The OPVs obtained a PCE of 19.2% (certified 18.8%), which achieved efficient charge generation and reduced  $V_{OC}$  loss. Liu et al. developed wide bandgap polymers based on D-A alternating, named reg-PThE-1F, by introducing fluoro and carboxylate substituents in co-ordination [112]. The polymer shows a wide absorption scope of 300 to 600 nm. There are two characteristic vibronic absorption peaks that are situated at about 570 and 520 nm, respectively, which suggests the highly aggregated feature of the polymer backbones. Introducing fluorine atoms enables a reduction in the energy levels of the polymer donors, which creates a higher OPV  $V_{OC}$ . The PCEs of ternary OPVs can reach 18.64% when introducing reg-PThE-1F into the D18:L8-BO binary system.

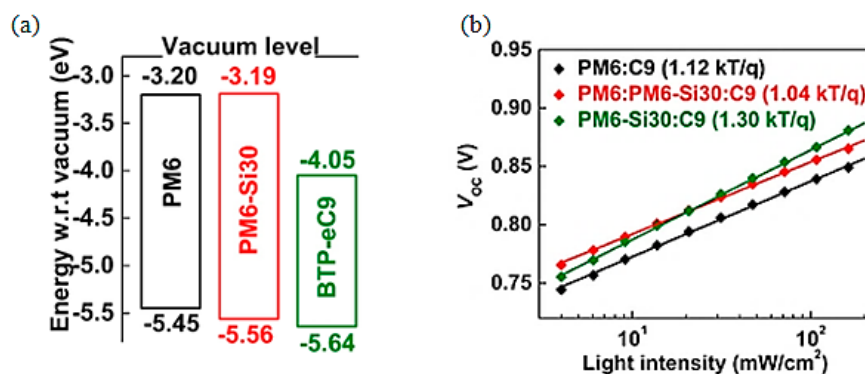


**Figure 11.** (a) The energy levels of PM6, PM6-Si30, and C9; (b) light intensity dependence of  $V_{OC}$  for the optimized binary and ternary OPVs; reproduced from [31].

#### 4.3.3. Reduce Losses

The  $E_{\text{loss}}$  of efficient OPVs is much greater than that of silicon and perovskite batteries and has been considered one of the main limiting factors for the development of OPVs. The ternary strategy can also be used to modulate phase separation morphology and reduce loss. The  $V_{OC}$  of ternary OPVs is usually limited to  $\sim 0.9$  V, which is significantly lower than

that of perovskite and silicon batteries. The low  $V_{OC}$  in OPVs is mainly due to high  $E_{loss}$ . Reducing  $E_{loss}$  is the key to further improving the performance of OPVs. The  $E_{loss}$  in OPVs comes from the three parts shown in Equation (1), where  $\Delta E_{CT}$  is the gap between the charge transfer energy level ( $E_{CT}$ ) and optical band gap ( $E_g^{opt}$ ), as shown in Equation (2);  $\Delta E_{nr}$  and  $\Delta E_r$  refer to the energy losses caused by nonradiative and radiative recombination, respectively. [111,123] The  $\Delta E_r$  is inevitable in OPVs, leaving no room for adjustment.

$$E_{loss} = \Delta E_{CT} + \Delta E_{nr} + \Delta E_r, \quad (1)$$

$$\Delta E_{CT} = E_g^{opt} + E_{CT}, \quad (2)$$

$$\Delta E_{nr} = -k_B T \ln EQE_{ET}, \quad (3)$$

The study has suggested that the  $\Delta E_{CT}$  can be low to negligible when the HOMO levels of NFAs and polymer donors are almost the same. High-performance OPVs with a high  $V_{OC}$  and low band gap can be manufactured by introducing conjugated small molecules with adverse energy level alignments. In 2021, An et al. designed a conjugated polymer based on thiadiazole named PB2F [111]. The polymer possesses a wide bandgap of 2.12 eV, a high  $EQE_{ET}$  of  $3.9 \times 10^{-3}$ , and a deep HOMO level of  $-5.64$  eV in a neat film. PB2F takes advantage of the third component to decrease the  $E_{loss}$  (0.559 eV) of the OPVs based on PBDB-TF:BTP-eC9, and  $\Delta E_{CT}$  (0.056 eV) and  $\Delta E_{nr}$  (0.231 eV) can also be simultaneously reduced. The  $V_{OC}$  of ternary OPVs improved gradually along with ascending PB2F content. The  $EQE_{ET}$  of optimal ternary OPVs increases from  $1.3 \times 10^{-4}$  to  $2.2 \times 10^{-4}$ , corresponding to  $\Delta E_{nr}$  reduced by 0.013 eV; the  $\Delta E_{CT}$  decreased by 0.011 eV. The  $V_{OC}$  of ternary OPVs is 0.021 V higher than that of the binary OPVs. The OPVs demonstrated a PCE of 18.6% under the optimal ratio of PBDB-TF:PB2F:BTP-eC9. A new NFAs acceptor named BTP-F was synthesized by Cai et al. [108]. BTP-F was introduced into the PM6:BTP-eC9 blend film. The strength of EQE is enhanced in the absorption scope of 450–800 nm by adding the BTP-F, which achieved a high  $J_{SC}$  in ternary OPVs. BTP-F and BTP-eC9 formed well-mixed acceptor phases in ternary blends. The  $\Delta E_{nr}$  in ternary OPVs was suppressed by adding BTP-F. The  $V_{loss}$  values are 0.517, 0.540, and 0.549 V for the PM6:BTP-F, PM6:BTP-eC9:BTP-F, and PM6:BTP-eC9, respectively. The  $EQE_{ET}$  values of PM6:BTP-F, PM6:BTP-eC9:BTP-F, and PM6:BTP-eC9 are  $6.00 \times 10^{-4}$ ,  $3.66 \times 10^{-4}$ , and  $2.35 \times 10^{-4}$ , respectively. The corresponding voltage losses of the nonradiative recombination ( $\Delta V_{nr}$ ) values are 0.185, 0.198, and 0.209 V for the PM6:BTP-F, PM6:BTP-eC9:BTP-F, and PM6:BTP-eC9-based OPVs, respectively. The PM6:BTP-eC9:BTP-F-based OPVs reached a PCE of 18.45% after adding 15 wt% BTP-F. Sun et al. developed NFA ZY-4Cl, which formed cascade LUMO energy levels and possessed a complementary absorption profile with the PM6:BTP-eC9 blend [116]. The ternary blends have a reduced trap state density, inhibited nonradiative recombination, and improved molecular order when compared to the binary blends, resulting in relatively low  $V_{loss}$  when compared to either of the binary blends. The density of trap state ( $n_t$ ) can be determined by  $V_{TFL} = n_t L^2 / (2\epsilon\epsilon_0)$ , where  $V_{TFL}$  is the limit voltage of trap filling,  $L$  is active layer thickness,  $e$  is the basic charge,  $\epsilon$  is the relative dielectric constant, and  $\epsilon_0$  is the vacuum dielectric constant. The  $n_t$  of ternary OPVs is  $1.136 \times 10^{16} \text{ cm}^{-3}$ , which is reduced to  $1.089 \times 10^{16} \text{ cm}^{-3}$ . The  $V_{loss}$  of the ternary OPVs is relatively low (0.520 V) compared to that of the PM6:ZY-4Cl (0.679 V)- and PM6:BTP-eC9 (0.532 V)-based binary OPVs. The low  $V_{loss}$  of the ternary OPVs could be due to a low  $\Delta V_{nr}$ . The  $EQE_{ET}$  of the ternary OPVs is relatively high ( $3.7 \times 10^{-4}$ ) in comparison to that of PM6:BTP-eC9 ( $1.9 \times 10^{-4}$ )-based binary OPVs. The  $\Delta V_{nr}$  of ternary OPVs (0.198 V) is relatively low compared to that of the binary OPVs (0.214 V). This  $\Delta V_{nr}$  difference between ternary and PM6:BTP-eC9-based binary OPVs reached 0.016 V, which is very consistent with the  $V_{loss}$  difference (0.012 V) of these OPVs. The ternary OPVs achieved a PCE of 18.69% (certified as 18.2%) by adding 12 wt% ZY-4Cl. Min et al. synthesized an asymmetric acceptor named BTP-2F2Cl that was introduced to the PM1:L8-BO blend [120]. The calculated increased exciton diffusion length (LD) values are 7.03 nm, 6.33 nm, and 4.98 nm for BTP-2F2Cl,



L8-BO:BTP-2F2Cl, and L8-BO. The photo-induced exciton in the acceptor phase of an alloy can be diffused over further distances during an efficient exciton lifetime in comparison with the L8-BO film. These results allow ternary systems to have relatively low nonradiative recombination and relatively high luminescence quantum efficiencies, resulting in a relatively low  $E_{\text{loss}}$  when compared to that of the binary OPVs. A PCE achieved 19.17% (certified value 18.7%) for the ternary OPVs, with a FF of 80.14%,  $J_{\text{SC}}$  of 27.15 mA cm<sup>-2</sup>, and  $V_{\text{OC}}$  of 0.881 V. Improving exciton behavior is a significant method for reducing  $\Delta E_{\text{nr}}$  and achieving high-performance OPVs. Chen et al. constructed the ternary OPVs being made up of asymmetric BTP-S9 and symmetric BTP-eC9 acceptors with similar absorption spectra [124]. BTP-S9 has low energy disorder and high luminous efficiency due to two asymmetric terminals. The compatibility among the two acceptors can make use of the Flory-Huggins interaction parameter  $\chi_{\text{A1-A2}}$ . The  $\chi_{\text{A1-A2}}$  of BTP-S9 and BTP-eC9 is only 0.008, indicating that the two NFAs have good miscibility. Ternary OPVs have a relatively low  $E_{\text{loss}}$  (0.501 eV) compared to the two binary OPVs, which contributes to a relatively high  $V_{\text{OC}}$  in comparison to both binary OPVs. The reduction in the  $E_{\text{loss}}$  of ternary OPVs is due to a reduction in  $\Delta E_{\text{nr}}$  (0.203 eV) and  $\Delta E_{\text{r}}$  (0.048 eV) in comparison to the OPVs based on PM6:BTP-eC9. The OPVs based on PM6:BTP-S9 deliver a high EQE<sub>ET</sub> ( $4.71 \times 10^{-2}\%$ ), which is relatively high compared to the OPVs ( $1.78 \times 10^{-2}\%$ ) based on PM6:BTP-eC9. The EQE<sub>ET</sub> of ternary OPVs is  $2.95 \times 10^{-2}\%$ , measured between binary OPVs. The increased luminescence efficiency of the BTP-eC9:BTP-S9 composite results in a decreasing  $\Delta E_{\text{nr}}$  for ternary OPVs when compared with the PM6:BTP-eC9 composite. The ternary OPVs showed the lowest  $E_{\text{loss}}$  of the three types of OPVs, with a relatively high  $V_{\text{OC}}$  in comparison to both of the binary OPVs. The decrease in energy disturbance and the inhibition of nonradiative decay result in an increase in  $V_{\text{OC}}$ . The optimal ternary OPVs showed a PCE of 18.82%, with a  $V_{\text{OC}}$  of 0.861 V. The symmetric and asymmetric compound strategy can alleviate  $E_{\text{loss}}$  by adjusting luminescence efficiency and energetic disorder. Tan et al. reported an NFA named DTTC-4ClC9, selecting a dithienocyclopentacarbazole core as the third component [125]. The PCEs of OPVs based on PM6:BTP-BO-4Cl:DTTC-4ClC9 increased from 17.11% to 18.21%, and the  $V_{\text{OC}}$ ,  $J_{\text{SC}}$ , and FF increased simultaneously when adding 15 wt% DTTC-4ClC9. The  $\Delta E_{\text{nr}}$  of OPVs decreased to 0.207 eV, which led to reduced energy loss. Deeply understanding the exciton and carrier dynamic process for minimizing  $E_{\text{loss}}$  by using a ternary strategy should be an important research topic.

#### 4.3.4. Morphology Control

In addition to enhancing the capture ability of photons, adjusting energy levels, and reducing losses, morphology optimization also plays an important role in the performance of ternary OPVs. Morphology optimization mainly includes crystallinity, molecular stacking, molecular orientation, and domain sizes. Morphology optimization plays an important role in improving free carrier generation and charge transport performance, resulting in an improved FF value. Yan et al. showed a double-fibril network based on a ternary blend film, which is constructed by combining an NFA filament assembly and ancillary conjugated polymer crystallizers [122]. The obtained nanostructure can well satisfy efficient free charge transport and exciton dissociation. Exciton diffusion length reached 40 nm, free charge drift length reached 2700 nm, and free charge diffusion length reached 105 nm. Exciton diffusion length of the donor phase increased by 11% after the addition of D18 to PM6:L8-BO, which is caused by the increased crystallinity and diameter of the fibril by the optimized morphology. Transient absorption spectroscopy measurements were performed, and the kinetics were extracted for the three blends at 600 nm. PM6:L8-BO has the formation of a better mixing zone, and D18:L8-BO possesses a large NFA fibril diameter. The merit of the two binary blends was concentrated in the ternary blends, which achieved a PCE of 19.3% (certified 19.2%), resulting in high performance for  $J_{\text{SC}}$  and FF. A double-fibril network was demonstrated that makes the photoelectric parameters match well with the length of morphological features and makes good use of excitons and free charges. It also brings about decreasing recombination ratios and increasing exciton



diffusion lengths. The photon-to-electron losses were the smallest in the ternary OPVs in comparison to that of their binary OPVs. The highly crystalline polymer D18 enhances the crystallinity of blend films and retains the main PM6:L8-BO morphology framework. Conjugated polymer donors with deep HOMO levels are significant for improving the PCEs of OPVs via reducing photovoltage loss and ensuring good BHJ morphology in OPVs. Zhang et al. prepared ternary OPVs by selecting two chlorinated and fluorinated acceptors (eC9-2Cl and L8-BO) with similar chemical constitutions [13]. The  $J_{SC}$ ,  $V_{OC}$ , and FF of OPVs showed a slight increase, along with an increase in the eC9-2Cl content. The EQE values mildly improved, along with the increase in eC9-2Cl content in the acceptors to 30 wt%. The spectral difference ( $\Delta EQE$ ) ( $\Delta EQE$  value is greater than zero) appeared between the binary OPVs and the optimum ternary OPVs based on L8-BO, which indicated that the exciton utilization efficiency improved in the optimized ternary OPVs. The  $\eta_{CT}$  and the  $P_{coll}$  of OPVs based on L8-BO:eC9-2Cl, eC9-2Cl, and L8-BO were 98.21%/89.38%, 96.48%/87.69%, and 97.73%/88.42%, respectively. The  $J_{SC}$  and FF increased in the optimum ternary OPVs because of an improvement in  $\eta_{CT}$  and  $P_{coll}$ . The optimal ternary OPVs achieve a PCE of 18.66% with a  $J_{SC}$  of 26.63 mA cm<sup>-2</sup>,  $V_{OC}$  of 0.89 V, and an FF of 78.74%. The realization of efficient ternary OPVs can also combine the advantages of chlorinated and fluorinated NFAs [13]. Xu et al. developed two Y-series NFAs by introducing 2D side chains named BTP-FTh and BTP-Th [93]. BTP-FTh has relatively good electron mobility and crystallinity in comparison to BTP-Th. DTT as an additive and IDIC as the second acceptor can enhance charge extraction, optimize the crystallinity of the blend morphology, and gradually inhibit charge recombination. Femtosecond transient absorption spectroscopy (fs-TAS) was used to detect photo-induced electron and hole transfer dynamics in the best ternary blend containing 10 wt% DTT and PTQ10:BTP-FTh film. The optimization of the PTQ10:BTP-FTh:IDIC (DTT) blend exhibited a long exciton diffusion time ( $44.5 \pm 8.4$  ps) and mildly improved hole transfer constant ( $0.84 \pm 0.09$  ps), which indicated the formation of large pure acceptor domain and reduced mixed-phase, resulting in high charge extraction and free charge carrier lifetimes. The  $J_{SC}$  vs. incident light intensity ( $P_{light}$ ) diagrams can be used to evaluate the bimolecular charge recombination for OPVs, which follows the function of  $J_{SC} \propto P_{light}^\alpha$ . The  $\alpha$  value increased from 0.991 to 0.995 for the ternary blend OPVs based on PTQ10:BTP-FTh:IDIC (DTT). The optimal PTQ10:BTP-FTh:IDIC (DTT) OPVs achieved high charge carrier mobility. The  $\mu_e/\mu_h$  ratio is the most balanced (1.04), which was beneficial to the inhibition of the charge recombination. The FF of PTQ10:BTP-FTh binary OPVs were improved stepwise from 76.7% to 78.6% by the addition of IDIC and increased to 80.6% by the addition of DTT. With the addition of IDIC and DTT into the host blend, based on PTQ10:BTP-FTh, the  $J_{SC}$  (27.17 mA cm<sup>-2</sup>) and  $V_{OC}$  (0.870 V) were enhanced because of the increase in the LUMO level and the improvement in charge extraction, with the PCEs reaching 19.05%. Zhang et al. reported asymmetric NFAs named AITC, which showed a wide absorption scope of 500–700 nm and a large dipole moment to strengthen the molecular packing of the BTP-eC9 and PM6 [117]. The miscibility of BTP-eC9 and AITC was studied in the light of the Flory-Huggins interaction parameter ( $\chi$ ) ( $\chi \propto (\sqrt{\gamma_{IDT6-T}} - \sqrt{\gamma_{BTP-eC9}})^2$ ) by the surface free energy ( $\gamma_{BTP-eC9}$  and  $\gamma_{AITC}$ ). The  $\chi$  of AITC:BTP-eC9 is 0.05 mN m<sup>-1</sup> using the parameters of AITC and BTP-eC9, which suggested the easy formation of hybrid acceptor phases in AITC:BTP-eC9 blends. The face-on orientations of the AITC:BTP-eC9, AITC, and BTP-eC9 films suggested  $\pi$ - $\pi$  stacking peaks at 1.757 Å<sup>-1</sup> (d-spacing is 3.574 Å), 1.763 Å<sup>-1</sup> (3.562 Å), and 1.745 Å<sup>-1</sup> (3.599 Å), respectively. The enhanced molecular packing decreased the active energy of the charge recombination, exciton dissociation, and  $\Delta E_{nr}$ ; the PCE of the ternary OPVs reached 18.8%. The PCEs of tandem OPVs based on a BHJ at the bottom of PM6:AITC and a BHJ at the top of PM6:AITC:BTP-eC9 reached 19.4%. The appropriate third variable is particularly important in changing the morphology. The formation of suitable molecular fillers and three-dimensional charge paths through the ternary strategy is the key to improving the PCE of the three-component system.

The change in molecular properties over time is the main factor controlling OPV operation. The relationship between the properties of OPV and molecular properties is as follows: molecular properties (photochemical stability) → morphological properties (morphological stability) → OPVs properties (electrical stability) in the corresponding order of influence. Morphological stability has a significant effect on the carrier dynamics of OPVs, including exciton dissociation, charge transport, and recombination. The strategies to improve the morphological stability of the active layer include improving molecular compatibility and forming a ternary structure for the crosslinked active layer. Higher mixing entropy can be obtained by adding the third component. The morphological stability can also be improved by a third polymer component. Chu et al. prepared efficient thick-film OPVs with excellent flexibility using a ternary strategy and a functional bonding additive. Chu et al. added a novel wide band gap polymer donor, PBB1-F, with good planeness as a third component to a well-performing host system (PM6:Y6-BO-4Cl and PM6:BTP-eC9) to optimize the molecular superposition and morphology of the active layer [91]. As an additive, polyarene ether not only improves exciton ionization efficiency but also effectively enhances domain interaction as a locking substrate, improving the mechanical stability of the active layer. The interaction between the third component and the additive and the molecule is enhanced, which is effective at improving the morphology stability.

## 5. Summary and Perspectives

The remarkable development of OPVs has been achieved, along with the exploration of various functional layer materials and device engineering. PCEs of over 19% have been obtained in the state-of-the-art single junction OPVs. The next stage will make the technology more suitable for commercialization and scale as the performance of OPVs continues to improve. There is still a long way to go to achieve widespread application. Several key issues and research areas need to be further studied.

(i) The balance between  $J_{SC}$  and  $V_{OC}$  has always been a hot research topic. A higher  $V_{OC}$  can be obtained at deeper HOMO levels. Meanwhile, with an increase in band gap, light absorption decreases, resulting in a decrease in  $J_{SC}$ , which ultimately affects PCE. Molecular engineering and material matching should be the potential way to solve the problem.

(ii) Minimizing energy loss should be one of the key factors for pushing the further performance improvement of OPVs. NFAs possess relatively low energetic disorder and, therefore, sharper absorption onsets. Further innovation on NFAs should be considered, which may provide a means to realize the minimized voltage loss of OPVs. From the perspective of device engineering, the ternary strategy has been demonstrated as an important technology for reducing energy loss. Further explorations of ternary OPVs should focus on an in-depth working mechanism for realizing the comprehensive optimization of dynamic exciton and carrier processes.

(iii) With the continuous development of OPVs, people should pay more attention to improving the stability of OPVs, in addition to improving the efficiency of OPVs. The single-component-molecule-based OPVs usually possess superior photo-stability and thermal stability than the widely explored D:A mixture system, which should also be a focus in future research directions.

(iv) Low-cost production is also more in line with future commercialization goals and can be achieved by building the key building blocks of polymer donors or NFAs with simple structures while developing synthetic routes that avoid toxic reagents and secondary products.

(v) The fabrication process matched with future commercial production should also be considered. The use of LbL processing methods should facilitate the formation of quasi-planar or interdigitated heterojunctions to achieve vertical phase separation. At the same time, the LbL processing method is more suitable for mass production in the future. From

the point of view of device engineering, the further study of LbL OPVs is a promising way to drive performance improvement.

**Author Contributions:** Conceptualization, C.X., W.X. and Z.L.; writing—original draft preparation, H.T. and M.Z. (Mingxin Zhao); writing—review and editing, X.M., M.Z. (Miao Zhang) and F.Z.; supervision, F.Z. All authors have read and agreed to the published version of the manuscript.

**Funding:** This work was supported by the Fundamental Research Funds for the Central Universities (2022JBZY002), the National Natural Science Foundation of China (62105017, 62205276, 62175011, 61975006) and the National Natural Science Foundation of China-Swedish Foundation for International Cooperation in Research and Higher education.

**Data Availability Statement:** No new data were created or analyzed in this study.

**Acknowledgments:** The authors also want to thank Beijing Jiaotong University for all the support.

**Conflicts of Interest:** The authors declare no conflict of interest.

## References

1. Xu, W.; Chang, Y.; Zhu, X.; Wei, Z.; Zhang, X.; Sun, X.; Lu, K.; Wei, Z. Organic solar cells based on small molecule donor and polymer acceptor. *Chin. Chem. Lett.* **2022**, *33*, 123–132. [\[CrossRef\]](#)
2. Liu, Y.; Li, B.; Ma, C.-Q.; Huang, F.; Feng, G.; Chen, H.; Hou, J.; Yan, L.; Wei, Q.; Luo, Q. Recent progress in organic solar cells (Part I material science). *Sci. China Chem.* **2022**, *65*, 224–268. [\[CrossRef\]](#)
3. Li, H.; Lu, K.; Wei, Z. Polymer/small molecule/fullerene based ternary solar cells. *Adv. Energy Mater.* **2017**, *7*, 1602540. [\[CrossRef\]](#)
4. Tang, C.W. Two-layer organic photovoltaic cell. *Appl. Phys. Lett.* **1986**, *48*, 183–185. [\[CrossRef\]](#)
5. Yu, G.; Gao, J.; Hummelen, J.C.; Wudl, F.; Heeger, A.J. Polymer photovoltaic cells: Enhanced efficiencies via a network of internal donor-acceptor heterojunctions. *Science* **1995**, *270*, 1789–1791. [\[CrossRef\]](#)
6. Gasparini, N.; Salleo, A.; McCulloch, I.; Baran, D. The role of the third component in ternary organic solar cells. *Nat. Rev. Mater.* **2019**, *4*, 229–242. [\[CrossRef\]](#)
7. Lin, Y.; Wang, J.; Zhang, Z.G.; Bai, H.; Li, Y.; Zhu, D.; Zhan, X. An electron acceptor challenging fullerenes for efficient polymer solar cells. *Adv. Mater.* **2015**, *27*, 1170–1174. [\[CrossRef\]](#)
8. Yuan, J.; Zhang, Y.; Zhou, L.; Zhang, G.; Yip, H.-L.; Lau, T.-K.; Lu, X.; Zhu, C.; Peng, H.; Johnson, P.A. Single-junction organic solar cell with over 15% efficiency using fused-ring acceptor with electron-deficient core. *Joule* **2019**, *3*, 1140–1151. [\[CrossRef\]](#)
9. Ma, X.; Jiang, Q.; Xu, W.; Xu, C.; Jeong, S.Y.; Woo, H.Y.; Wu, Q.; Zhang, X.; Yuan, G.; Zhang, F. Layered optimization strategy enables over 17.8% efficiency of layer-by-layer organic photovoltaics. *Chem. Eng. J.* **2022**, *442*, 136368. [\[CrossRef\]](#)
10. Gao, J.; Wang, J.; An, Q.; Ma, X.; Hu, Z.; Xu, C.; Zhang, X.; Zhang, F. Over 16.7% efficiency of ternary organic photovoltaics by employing extra PC<sub>71</sub>BM as morphology regulator. *Sci. China Chem.* **2020**, *63*, 83–91. [\[CrossRef\]](#)
11. Jiang, M.; Zhi, H.-F.; Zhang, B.; Yang, C.; Mahmood, A.; Zhang, M.; Woo, H.Y.; Zhang, F.; Wang, J.-L.; An, Q. Controlling Morphology and Voltage Loss with Ternary Strategy Triggers Efficient All-Small-Molecule Organic Solar Cells. *ACS Energy Lett.* **2023**, *8*, 1058–1067. [\[CrossRef\]](#)
12. Ma, X.; Zeng, A.; Gao, J.; Hu, Z.; Xu, C.; Son, J.H.; Jeong, S.Y.; Zhang, C.; Li, M.; Wang, K. Approaching 18% efficiency of ternary organic photovoltaics with wide bandgap polymer donor and well compatible Y6: Y6-1O as acceptor. *Nat. Sci. Rev.* **2021**, *8*, nwaa305. [\[CrossRef\]](#) [\[PubMed\]](#)
13. Zhang, S.; Ma, X.; Niu, L.; Jeong, S.Y.; Woo, H.Y.; Zhou, Z.; Zhang, F. 18.66% Efficiency of Polymer Solar Cells Employing Two Nonfullerene Acceptors with Fluorine or Chlorine Substitution. *Sol. RRL* **2023**, *7*, 2200957. [\[CrossRef\]](#)
14. Gao, J.; Ma, X.; Xu, C.; Wang, X.; Son, J.H.; Jeong, S.Y.; Zhang, Y.; Zhang, C.; Wang, K.; Niu, L. Over 17.7% efficiency ternary-blend organic solar cells with low energy-loss and good thickness-tolerance. *Chem. Eng. J.* **2022**, *428*, 129276. [\[CrossRef\]](#)
15. Fan, Q.; Lin, F.R.; Ma, W.; Jen, A.K.-Y. Selenium-fused Y6 derivatives and their derived polymerized small molecule acceptors for efficient organic solar cells. *Sci. China Chem.* **2022**, *66*, 615–619. [\[CrossRef\]](#)
16. Wang, X.; Sun, Q.; Gao, J.; Ma, X.; Son, J.H.; Jeong, S.Y.; Hu, Z.; Niu, L.; Woo, H.Y.; Zhang, J. Ternary organic photovoltaic cells exhibiting 17.59% efficiency with two compatible Y6 derivations as acceptor. *Sol. RRL* **2021**, *5*, 2100007. [\[CrossRef\]](#)
17. Li, X.; Luo, S.; Sun, H.; Sung, H.H.-Y.; Yu, H.; Liu, T.; Xiao, Y.; Bai, F.; Pan, M.; Lu, X. Medium band-gap non-fullerene acceptors based on a benzothiophene donor moiety enabling high-performance indoor organic photovoltaics. *Energy Environ. Sci.* **2021**, *14*, 4555–4563. [\[CrossRef\]](#)
18. Gao, J.; Yu, N.; Chen, Z.; Wei, Y.; Li, C.; Liu, T.; Gu, X.; Zhang, J.; Wei, Z.; Tang, Z. Over 19.2% Efficiency of Organic Solar Cells Enabled by Precisely Tuning the Charge Transfer State Via Donor Alloy Strategy. *Adv. Sci.* **2022**, *9*, 2203606. [\[CrossRef\]](#)
19. Li, G.; Zhu, R.; Yang, Y. Polymer solar cells. *Nat. Photonics* **2012**, *6*, 153–161. [\[CrossRef\]](#)
20. Pan, Y.Q.; Sun, G.Y. Star-Shaped Non-Fullerene Small Acceptors for Organic Solar Cells. *ChemSusChem* **2019**, *12*, 4570–4600. [\[CrossRef\]](#)
21. Zhao, C.C.; Wang, J.X.; Zhao, X.Y.; Du, Z.L.; Yang, R.Q.; Tang, J.G. Recent advances, challenges and prospects in ternary organic solar cells. *Nanoscale* **2021**, *13*, 2181–2208. [\[CrossRef\]](#)

22. Armin, A.; Li, W.; Sandberg, O.J.; Xiao, Z.; Ding, L.M.; Nelson, J.; Neher, D.; Vandewal, K.; Shoaee, S.; Wang, T.; et al. A History and Perspective of Non-Fullerene Electron Acceptors for Organic Solar Cells. *Adv. Energy Mater.* **2021**, *11*, 2003570. [\[CrossRef\]](#)
23. Wang, G.; Melkonyan, F.S.; Facchetti, A.; Marks, T.J. All-Polymer Solar Cells: Recent Progress, Challenges, and Prospects. *Angew. Chem. Inter. Ed.* **2019**, *58*, 4129–4142. [\[CrossRef\]](#) [\[PubMed\]](#)
24. Xiong, J.; Jin, K.; Jiang, Y.; Qin, J.; Wang, T.; Liu, J.; Liu, Q.; Peng, H.; Li, X.; Sun, A. Thiolactone copolymer donor gifts organic solar cells a 16.72% efficiency. *Sci. Bull.* **2019**, *64*, 1573–1576. [\[CrossRef\]](#)
25. Qin, J.; Zhang, L.; Zuo, C.; Xiao, Z.; Yuan, Y.; Yang, S.; Hao, F.; Cheng, M.; Sun, K.; Bao, Q. A chlorinated copolymer donor demonstrates a 18.13% power conversion efficiency. *J. Semicond.* **2021**, *42*, 010501. [\[CrossRef\]](#)
26. Wang, X.; Xiao, C.; Sun, X.; Saparbaev, A.; Lei, S.; Zhang, M.; Zhong, T.; Li, Z.; Zhang, J.; Zhang, M. Hammer throw-like hybrid cyclic and alkyl chains: A new side chain engineering for over 18% efficiency organic solar cells. *Nano Energy* **2022**, *101*, 107538. [\[CrossRef\]](#)
27. Zhang, M.; Guo, X.; Ma, W.; Ade, H.; Hou, J. A large-bandgap conjugated polymer for versatile photovoltaic applications with high performance. *Adv. Mater.* **2015**, *27*, 4655–4660. [\[CrossRef\]](#) [\[PubMed\]](#)
28. Zhang, S.; Qin, Y.; Zhu, J.; Hou, J. Over 14% Efficiency in Polymer Solar Cells Enabled by a Chlorinated Polymer Donor. *Adv. Mater.* **2018**, *30*, 1800868. [\[CrossRef\]](#) [\[PubMed\]](#)
29. Yang, T.; Liao, C.; Duan, Y.; Xu, X.; Deng, M.; Yu, L.; Li, R.; Peng, Q. Tradeoff between Intermolecular Interaction and Backbone Disorder by High Molecular Dipole Block for Improving Blend Morphology of Polymer Solar Cells. *Adv. Funct. Mater.* **2022**, *32*, 2208950. [\[CrossRef\]](#)
30. Lu, H.; Wang, H.; Ran, G.; Li, S.; Zhang, J.; Liu, Y.; Zhang, W.; Xu, X.; Bo, Z. Random Terpolymer Enabling High-Efficiency Organic Solar Cells Processed by Nonhalogenated Solvent with a Low Nonradiative Energy Loss. *Adv. Funct. Mater.* **2022**, *32*, 2203193. [\[CrossRef\]](#)
31. Peng, W.; Lin, Y.; Jeong, S.Y.; Genene, Z.; Magomedov, A.; Woo, H.Y.; Chen, C.; Wahyudi, W.; Tao, Q.; Deng, J. Over 18% ternary polymer solar cells enabled by a terpolymer as the third component. *Nano Energy* **2022**, *92*, 106681. [\[CrossRef\]](#)
32. Zhou, L.; Meng, L.; Zhang, J.; Qin, S.; Zhang, J.; Li, X.; Li, J.; Wei, Z.; Li, Y. Terpolymer Donor with Inside Alkyl Substituents on Thiophene  $\pi$ -Bridges toward Thiazolothiazole A2-Unit Enables 18.21% Efficiency of Polymer Solar Cells. *Adv. Sci.* **2022**, *9*, 2203513. [\[CrossRef\]](#) [\[PubMed\]](#)
33. Zhou, L.; Meng, L.; Zhang, J.; Zhu, C.; Qin, S.; Angunawela, I.; Wan, Y.; Ade, H.; Li, Y. Introducing Low-Cost Pyrazine Unit into Terpolymer Enables High-Performance Polymer Solar Cells with Efficiency of 18.23%. *Adv. Funct. Mater.* **2022**, *32*, 2109271. [\[CrossRef\]](#)
34. Liao, Z.; Hu, D.; Tang, H.; Huang, P.; Singh, R.; Chung, S.; Cho, K.; Kumar, M.; Hou, L.; Chen, Q. 18.42% efficiency polymer solar cells enabled by terpolymer donors with optimal miscibility and energy levels. *J. Mater. Chem. A* **2022**, *10*, 7878–7887. [\[CrossRef\]](#)
35. Sun, C.; Pan, F.; Bin, H.; Zhang, J.; Xue, L.; Qiu, B.; Wei, Z.; Zhang, Z.-G.; Li, Y. A low cost and high performance polymer donor material for polymer solar cells. *Nat. Commun.* **2018**, *9*, 743. [\[CrossRef\]](#) [\[PubMed\]](#)
36. Li, S.; Ding, Y.; Xu, L.; Zhao, W.; Zhang, J.; Qin, J.; Zhang, Y.; Zhao, J.; He, C.; Peng, Q.; et al. The Key Role of Subtle Substitution for a High-Performance Ester-Modified Oligothiophene-Based Polymer Used in Photovoltaic Cells. *Chin. J. Chem.* **2022**, *40*, 2867–2874. [\[CrossRef\]](#)
37. Yuan, X.Y.; Zhao, Y.L.; Xie, D.S.; Pan, L.H.; Liu, X.Y.; Duan, C.H.; Huang, F.; Cao, Y. Polythiophenes for organic solar cells with efficiency surpassing 17%. *Joule* **2022**, *6*, 647–661. [\[CrossRef\]](#)
38. Xu, Y.; Cui, Y.; Yao, H.; Zhang, T.; Zhang, J.; Ma, L.; Wang, J.; Wei, Z.; Hou, J. A new conjugated polymer that enables the integration of photovoltaic and light-emitting functions in one device. *Adv. Mater.* **2021**, *33*, 2101090. [\[CrossRef\]](#)
39. Zhang, T.; An, C.; Cui, Y.; Zhang, J.; Bi, P.; Yang, C.; Zhang, S.; Hou, J. A universal nonhalogenated polymer donor for high-performance organic photovoltaic cells. *Adv. Mater.* **2022**, *34*, 2105803. [\[CrossRef\]](#)
40. Jiang, Q.; Han, P.; Ning, H.; Jiang, J.; Chen, H.; Xiao, Y.; Ye, C.-R.; Chen, J.; Lin, M.; He, F. Reducing steric hindrance around electronegative atom in polymer simultaneously enhanced efficiency and stability of organic solar cells. *Nano Energy* **2022**, *101*, 107611. [\[CrossRef\]](#)
41. Cao, J.; Yi, L.; Ding, L. The origin and evolution of Y6 structure. *J. Semicond.* **2022**, *43*, 030202. [\[CrossRef\]](#)
42. Zhang, J.; Bai, F.; Angunawela, I.; Xu, X.; Luo, S.; Li, C.; Chai, G.; Yu, H.; Chen, Y.; Hu, H. Alkyl-chain branching of non-fullerene acceptors flanking conjugated side groups toward highly efficient organic solar cells. *Adv. Energy Mater.* **2021**, *11*, 2102596. [\[CrossRef\]](#)
43. Li, C.; Zhou, J.; Song, J.; Xu, J.; Zhang, H.; Zhang, X.; Guo, J.; Zhu, L.; Wei, D.; Han, G. Non-fullerene acceptors with branched side chains and improved molecular packing to exceed 18% efficiency in organic solar cells. *Nat. Energy* **2021**, *6*, 605–613. [\[CrossRef\]](#)
44. Luo, Z.; Gao, Y.; Lai, H.; Li, Y.; Wu, Z.; Chen, Z.; Sun, R.; Ren, J.; He, F. Asymmetric side-chain substitution enables a 3D network acceptor with hydrogen bond assisted crystal packing and enhanced electronic coupling for efficient organic solar cells. *Energy Environ. Sci.* **2022**, *15*, 4601–4611. [\[CrossRef\]](#)
45. Chen, S.; Feng, L.; Jia, T.; Jing, J.; Hu, Z.; Zhang, K.; Huang, F. High-performance polymer solar cells with efficiency over 18% enabled by asymmetric side chain engineering of non-fullerene acceptors. *Sci. China Chem.* **2021**, *64*, 1192–1199. [\[CrossRef\]](#)
46. Cui, Y.; Yao, H.; Zhang, J.; Xian, K.; Zhang, T.; Hong, L.; Wang, Y.; Xu, Y.; Ma, K.; An, C. Single-junction organic photovoltaic cells with approaching 18% efficiency. *Adv. Mater.* **2020**, *32*, 1908205. [\[CrossRef\]](#) [\[PubMed\]](#)



47. Wang, L.; Guo, C.; Zhang, X.; Cheng, S.; Li, D.; Cai, J.; Chen, C.; Fu, Y.; Zhou, J.; Qin, H. Alkyl chain tuning of non-fullerene electron acceptors toward 18.2% efficiency binary organic solar cells. *Chem. Mater.* **2021**, *33*, 8854–8862. [\[CrossRef\]](#)
48. Chen, H.; Zou, Y.; Liang, H.; He, T.; Xu, X.; Zhang, Y.; Ma, Z.; Wang, J.; Zhang, M.; Li, Q. Lowering the energy loss of organic solar cells by molecular packing engineering via multiple molecular conjugation extension. *Sci. China Chem.* **2022**, *65*, 1362–1373. [\[CrossRef\]](#)
49. Chen, H.; Liang, H.; Guo, Z.; Zhu, Y.; Zhang, Z.; Li, Z.; Cao, X.; Wang, H.; Feng, W.; Zou, Y. Central Unit Fluorination of Non-Fullerene Acceptors Enables Highly Efficient Organic Solar Cells with Over 18% Efficiency. *Angew. Chem. Int. Ed.* **2022**, *61*, e202209580.
50. Janjua, M.R.S.A. All-small-molecule organic solar cells with high fill factor and enhanced open-circuit voltage with 18.25% PCE: Physical insights from quantum chemical calculations. *Spectrochim. Acta. A Mol. Biomol. Spectrosc.* **2022**, *279*, 121487. [\[CrossRef\]](#)
51. He, C.; Bi, Z.; Chen, Z.; Guo, J.; Xia, X.; Lu, X.; Min, J.; Zhu, H.; Ma, W.; Zuo, L. Compromising charge generation and recombination with asymmetric molecule for high-performance binary organic photovoltaics with over 18% certified efficiency. *Adv. Funct. Mater.* **2022**, *32*, 2112511. [\[CrossRef\]](#)
52. Li, P.; Meng, X.; Jin, K.; Xu, Z.; Zhang, J.; Zhang, L.; Niu, C.; Tan, F.; Yi, C.; Xiao, Z. Banana-shaped electron acceptors with an electron-rich core fragment and 3D packing capability. *Carbon Energy* **2023**, *5*, e250. [\[CrossRef\]](#)
53. Wu, B.Q.; Li, Y.L.; Tian, S.Z.; Zhang, Y.; Pan, L.H.; Liu, K.Z.; Yang, M.Q.; Huang, F.; Cao, Y.; Duan, C.H. Regioregular Non-Fused Polymerized Small Molecular Acceptors Enabling Efficient All-Polymer Solar Cells. *Chin. J. Chem.* **2023**, *41*, 790–796. [\[CrossRef\]](#)
54. Luo, Z.; Liu, T.; Ma, R.; Xiao, Y.; Zhan, L.; Zhang, G.; Sun, H.; Ni, F.; Chai, G.; Wang, J.; et al. Precisely Controlling the Position of Bromine on the End Group Enables Well-Regular Polymer Acceptors for All-Polymer Solar Cells with Efficiencies over 15%. *Adv. Mater.* **2020**, *32*, 2005942. [\[CrossRef\]](#)
55. Wang, T.; Sun, R.; Wang, W.; Li, H.; Wu, Y.; Min, J. Highly Efficient and Stable All-Polymer Solar Cells Enabled by Near-Infrared Isomerized Polymer Acceptors. *Chem. Mater.* **2021**, *33*, 761–773. [\[CrossRef\]](#)
56. Yu, H.; Wang, Y.; Kim, H.K.; Wu, X.; Li, Y.; Yao, Z.; Pan, M.; Zou, X.; Zhang, J.; Chen, S.; et al. A Vinylene-Linker-Based Polymer Acceptor Featuring a Coplanar and Rigid Molecular Conformation Enables High-Performance All-Polymer Solar Cells with Over 17% Efficiency. *Adv. Mater.* **2022**, *34*, 2200361. [\[CrossRef\]](#) [\[PubMed\]](#)
57. Fan, B.; Gao, W.; Wu, X.; Xia, X.; Wu, Y.; Lin, F.; Fan, Q.; Lu, X.; Li, W.; Ma, W.; et al. Importance of structural hinderance in performance-stability equilibrium of organic photovoltaics. *Nat. Commun.* **2022**, *13*, 5946. [\[CrossRef\]](#) [\[PubMed\]](#)
58. Yang, R.; Tian, J.; Liu, W.; Wang, Y.; Chen, Z.; Russell, T.P.; Liu, Y. Nonconjugated Self-Doped Polymer Zwitterions as Efficient Interlayers for High Performance Organic Solar Cells. *Chem. Mater.* **2022**, *34*, 7293–7301. [\[CrossRef\]](#)
59. Sun, W.J.; Wang, Y.T.; Zhang, Y.; Sun, B.; Zhang, Z.Q.; Xiao, M.J.; Li, X.Y.; Huo, Y.; Xin, J.; Zhu, Q. A Cathode Interface Layer Based on 4, 5, 9, 10-Pyrene Diimide for Highly Efficient Binary Organic Solar Cells. *Angew. Chem. Int. Ed.* **2022**, *61*, e202208383. [\[CrossRef\]](#)
60. Qin, Y.; Chang, Y.; Zhu, X.; Gu, X.; Guo, L.; Zhang, Y.; Wang, Q.; Zhang, J.; Zhang, X.; Liu, X. 18.4% efficiency achieved by the cathode interface engineering in non-fullerene polymer solar cells. *Nano Today* **2021**, *41*, 101289. [\[CrossRef\]](#)
61. Meng, H.; Liao, C.; Deng, M.; Xu, X.; Yu, L.; Peng, Q. 18.77% efficiency organic solar cells promoted by aqueous solution processed cobalt (II) acetate hole transporting layer. *Angew. Chem.* **2021**, *133*, 22728–22735. [\[CrossRef\]](#)
62. Wang, J.; Cui, Y.; Xu, Y.; Xian, K.; Bi, P.; Chen, Z.; Zhou, K.; Ma, L.; Zhang, T.; Yang, Y. A New Polymer Donor Enables Binary All-Polymer Organic Photovoltaic Cells with 18% Efficiency and Excellent Mechanical Robustness. *Adv. Mater.* **2022**, *34*, 2205009. [\[CrossRef\]](#) [\[PubMed\]](#)
63. Guo, C.; Li, D.; Wang, L.; Du, B.; Liu, Z.X.; Shen, Z.; Wang, P.; Zhang, X.; Cai, J.; Cheng, S. Cold-aging and solvent vapor mediated aggregation control toward 18% efficiency binary organic solar cells. *Adv. Energy Mater.* **2021**, *11*, 2102000. [\[CrossRef\]](#)
64. Liu, Q.; Jiang, Y.; Jin, K.; Qin, J.; Xu, J.; Li, W.; Xiong, J.; Liu, J.; Xiao, Z.; Sun, K. 18% Efficiency organic solar cells. *Sci. Bull.* **2020**, *65*, 272–275. [\[CrossRef\]](#) [\[PubMed\]](#)
65. Zhang, X.; Li, C.; Xu, J.; Wang, R.; Song, J.; Zhang, H.; Li, Y.; Jing, Y.-N.; Li, S.; Wu, G. High fill factor organic solar cells with increased dielectric constant and molecular packing density. *Joule* **2022**, *6*, 444–457. [\[CrossRef\]](#)
66. Cheng, Y.; Huang, B.; Huang, X.; Zhang, L.; Kim, S.; Xie, Q.; Liu, C.; Heumüller, T.; Liu, Z.; Zhang, Y. Oligomer-Assisted Photoactive Layers Enable > 18% Efficiency of Organic Solar Cells. *Angew. Chem.* **2022**, *134*, e202200329. [\[CrossRef\]](#)
67. Hong, L.; Yao, H.; Cui, Y.; Bi, P.; Zhang, T.; Cheng, Y.; Zu, Y.; Qin, J.; Yu, R.; Ge, Z. 18.5% efficiency organic solar cells with a hybrid planar/bulk heterojunction. *Adv. Mater.* **2021**, *33*, 2103091. [\[CrossRef\]](#)
68. Li, C.; Gu, X.; Chen, Z.; Han, X.; Yu, N.; Wei, Y.; Gao, J.; Chen, H.; Zhang, M.; Wang, A. Achieving record-efficiency organic solar cells upon tuning the conformation of solid additives. *J. Am. Chem. Soc.* **2022**, *144*, 14731–14739. [\[CrossRef\]](#)
69. Li, Z.Y.; Liang, Y.F.; Qian, X.T.; Ying, L.; Cao, Y. Suppressing non-radiative loss via a low-cost solvent additive enables high-stable all-polymer solar cells with 16.13% efficiency. *Chem. Eng. J.* **2022**, *446*, 136877. [\[CrossRef\]](#)
70. Xie, Y.; Ryu, H.S.; Han, L.; Cai, Y.; Duan, X.; Wei, D.; Woo, H.Y.; Sun, Y. High-efficiency organic solar cells enabled by an alcohol-washable solid additive. *Sci. China Chem.* **2021**, *64*, 2161–2168. [\[CrossRef\]](#)
71. Qin, J.; Yang, Q.; Oh, J.; Chen, S.; Odunmbaku, G.O.; Ouedraogo, N.A.N.; Yang, C.; Sun, K.; Lu, S. Volatile Solid Additive-Assisted Sequential Deposition Enables 18.42% Efficiency in Organic Solar Cells. *Adv. Sci.* **2022**, *9*, 2105347. [\[CrossRef\]](#)
72. Song, J.; Zhu, L.; Li, C.; Xu, J.; Wu, H.; Zhang, X.; Zhang, Y.; Tang, Z.; Liu, F.; Sun, Y. High-efficiency organic solar cells with low voltage loss induced by solvent additive strategy. *Matter* **2021**, *4*, 2542–2552. [\[CrossRef\]](#)

73. Li, Z.; Peng, F.; Ying, L.; Quan, H.; Li, J.; Wang, X.; Wu, H.; Huang, F.; Cao, Y. Fine Tuning Miscibility of Donor/Acceptor through Solid Additives Enables All-Polymer Solar Cells with 15.6% Efficiency. *Sol. RRL* **2021**, *5*, 2100549. [\[CrossRef\]](#)
74. Ma, X.; Xu, W.; Liu, Z.; Jeong, S.Y.; Xu, C.; Zhang, J.; Woo, H.Y.; Zhou, Z.; Zhang, F. Over 18.1% Efficiency of Layer-by-Layer Polymer Solar Cells by Enhancing Exciton Utilization near the ITO Electrode. *ACS Appl. Mater. Interfaces* **2023**, *15*, 7247–7254. [\[CrossRef\]](#) [\[PubMed\]](#)
75. Liu, Z.; Ma, X.; Xu, W.; Zhang, S.; Xu, C.; Jeong, S.Y.; Woo, H.Y.; Zhou, Z.; Zhang, F. 15.28% efficiency of conventional layer-by-layer all-polymer solar cells superior to bulk heterojunction or inverted cells. *Chem. Eng. J.* **2022**, *450*, 138146. [\[CrossRef\]](#)
76. Xu, W.; Zhu, X.; Ma, X.; Zhou, H.; Li, X.; Jeong, S.Y.; Woo, H.Y.; Zhou, Z.; Sun, Q.; Zhang, F. Achieving 15.81% and 15.29% efficiency of all-polymer solar cells based on layer-by-layer and bulk heterojunction structures. *J. Mater. Chem. A* **2022**, *10*, 13492–13499. [\[CrossRef\]](#)
77. Xu, W.; Li, X.; Jeong, S.Y.; Son, J.H.; Zhou, Z.; Jiang, Q.; Woo, H.Y.; Wu, Q.; Zhu, X.; Ma, X. Achieving 17.5% efficiency for polymer solar cells via a donor and acceptor layered optimization strategy. *J. Mater. Chem. C* **2022**, *10*, 5489–5496. [\[CrossRef\]](#)
78. Xu, C.; Jin, K.; Xiao, Z.; Zhao, Z.; Yan, Y.; Zhu, X.; Li, X.; Zhou, Z.; Jeong, S.Y.; Ding, L. Efficient Semitransparent Layer-by-Layer Organic Photovoltaics via Optimizing Wide Bandgap and Narrow Absorption Polymer Layer Thickness. *Sol. RRL* **2022**, *6*, 2200308. [\[CrossRef\]](#)
79. Xu, W.; Zhang, M.; Ma, X.; Zhu, X.; Jeong, S.Y.; Woo, H.Y.; Zhang, J.; Du, W.; Wang, J.; Liu, X.; et al. Over 17.4% efficiency of layer-by-layer all-polymer solar cells by improving exciton utilization in acceptor layer. *Adv. Funct. Mater.* **2023**, *33*, 2215204. [\[CrossRef\]](#)
80. He, C.; Pan, Y.; Lu, G.; Wu, B.; Xia, X.; Ma, C.Q.; Chen, Z.; Zhu, H.; Lu, X.; Ma, W. Versatile Sequential Casting Processing for Highly Efficient and Stable Binary Organic Photovoltaics. *Adv. Mater.* **2022**, *34*, 2203379. [\[CrossRef\]](#)
81. Wei, Y.; Chen, Z.; Lu, G.; Yu, N.; Li, C.; Gao, J.; Gu, X.; Hao, X.; Lu, G.; Tang, Z. Binary organic solar cells breaking 19% via manipulating the vertical component distribution. *Adv. Mater.* **2022**, *34*, 2204718. [\[CrossRef\]](#)
82. Yu, K.; Song, W.; Ge, J.; Zheng, K.; Xie, L.; Chen, Z.; Qiu, Y.; Hong, L.; Liu, C.; Ge, Z. 18.01% Efficiency organic solar cell and 2.53% light utilization efficiency semitransparent organic solar cell enabled by optimizing PM6: Y6 active layer morphology. *Sci. China Chem.* **2022**, *65*, 1615–1622. [\[CrossRef\]](#)
83. Firdaus, Y.; Isikgor, F.; Nugraha, M.; Yengel, E.; Harrison, G.; Hallani, R.; El Labban, A.; Faber, H.; Ma, C.; Zheng, X. Self-assembled monolayer enables HTL-free organic solar cells with 18% efficiency and improved operational stability. *ACS Energy Lett.* **2020**, *5*, 2935–2944.
84. Liu, L.; Chen, S.; Qu, Y.; Gao, X.; Han, L.; Lin, Z.; Yang, L.; Wang, W.; Zheng, N.; Liang, Y. Nanographene–osmapentalayne complexes as a cathode interlayer in organic solar cells enhance efficiency over 18%. *Adv. Mater.* **2021**, *33*, 2101279. [\[CrossRef\]](#) [\[PubMed\]](#)
85. Deng, J.; Huang, B.; Li, W.; Zhang, L.; Jeong, S.Y.; Huang, S.; Zhang, S.; Wu, F.; Xu, X.; Zou, G. Ferroelectric Polymer Drives Performance Enhancement of Non-fullerene Organic Solar Cells. *Angew. Chem. Int. Ed.* **2022**, *61*, e202202177. [\[CrossRef\]](#) [\[PubMed\]](#)
86. Li, S.; Fu, Q.; Meng, L.; Wan, X.; Ding, L.; Lu, G.; Lu, G.; Yao, Z.; Li, C.; Chen, Y. Achieving over 18% Efficiency Organic Solar Cell Enabled by a ZnO-Based Hybrid Electron Transport Layer with an Operational Lifetime up to 5 Years. *Angew. Chem.* **2022**, *134*, e202207397.
87. Yu, J.; Liu, X.; Zhong, Z.; Yan, C.; Liu, H.; Fong, P.W.; Liang, Q.; Lu, X.; Li, G. Copper phosphotungstate as low cost, solution-processed, stable inorganic anode interfacial material enables organic photovoltaics with over 18% efficiency. *Nano Energy* **2022**, *94*, 106923. [\[CrossRef\]](#)
88. Kataria, M.; Chau, H.D.; Kwon, N.Y.; Park, S.H.; Cho, M.J.; Choi, D.H. Y-Series-Based Polymer Acceptors for High-Performance All-Polymer Solar Cells in Binary and Non-binary Systems. *ACS Energy Lett.* **2022**, *7*, 3835–3854. [\[CrossRef\]](#)
89. Lin, Y.; Magomedov, A.; Firdaus, Y.; Kaltsas, D.; El-Labban, A.; Faber, H.; Naphade, D.R.; Yengel, E.; Zheng, X.; Yarali, E. 18.4% organic solar cells using a high ionization energy self-assembled monolayer as hole-extraction interlayer. *ChemSusChem* **2021**, *14*, 3569–3578. [\[CrossRef\]](#)
90. Lin, Y.; Zhang, Y.; Zhang, J.; Marcinkas, M.; Malinauskas, T.; Magomedov, A.; Nugraha, M.I.; Kaltsas, D.; Naphade, D.R.; Harrison, G.T. 18.9% Efficient Organic Solar Cells Based on n-Doped Bulk-Heterojunction and Halogen-Substituted Self-Assembled Monolayers as Hole Extracting Interlayers. *Adv. Energy Mater.* **2022**, *12*, 2202503. [\[CrossRef\]](#)
91. Wang, J.; Han, C.; Han, J.; Bi, F.; Sun, X.; Wen, S.; Yang, C.; Yang, C.; Bao, X.; Chu, J. Synergetic Strategy for Highly Efficient and Super Flexible Thick-film Organic Solar Cells. *Adv. Energy Mater.* **2022**, *12*, 2201614. [\[CrossRef\]](#)
92. Zhang, S.; Bi, F.; Han, J.; Shang, C.; Kang, X.; Bao, X. Boosts charge utilization and enables high performance organic solar cells by marco-and micro-synergistic method. *Nano Energy* **2022**, *102*, 107742. [\[CrossRef\]](#)
93. Chong, K.; Xu, X.; Meng, H.; Xue, J.; Yu, L.; Ma, W.; Peng, Q. Realizing 19.05% efficiency polymer solar cells by progressively improving charge extraction and suppressing charge recombination. *Adv. Mater.* **2022**, *34*, 2109516. [\[CrossRef\]](#)
94. Jia, Z.; Ma, Q.; Meng, L.; Zhang, J.; Qin, S.; Chen, Z.; Li, X.; Zhang, J.; Li, J.; Zhang, Z. Medium Bandgap Small Molecule Acceptors With Isomer-Free Chlorinated End Groups Enabling High-Performance Tandem Organic Solar Cells. *Adv. Funct. Mater.* **2022**, *32*, 2204720. [\[CrossRef\]](#)
95. Xiao, B.; Wu, H.; Cao, Y. Solution-processed cathode interfacial layer materials for high-efficiency polymer solar cells. *Mater. Today* **2015**, *18*, 385–394. [\[CrossRef\]](#)



96. Yang, Y.; Chen, W.; Dou, L.; Chang, W.-H.; Duan, H.-S.; Bob, B.; Li, G.; Yang, Y. High-performance multiple-donor bulk heterojunction solar cells. *Nat. Photonics* **2015**, *9*, 190–198. [\[CrossRef\]](#)
97. Lu, L.; Kelly, M.A.; You, W.; Yu, L. Status and prospects for ternary organic photovoltaics. *Nat. Photonics* **2015**, *9*, 491–500. [\[CrossRef\]](#)
98. Liu, F.; Zhou, L.; Liu, W.; Zhou, Z.; Yue, Q.; Zheng, W.; Sun, R.; Liu, W.; Xu, S.; Fan, H. Organic solar cells with 18% efficiency enabled by an alloy acceptor: A two-in-one strategy. *Adv. Mater.* **2021**, *33*, 2100830. [\[CrossRef\]](#) [\[PubMed\]](#)
99. Zhan, L.; Li, S.; Xia, X.; Li, Y.; Lu, X.; Zuo, L.; Shi, M.; Chen, H. Layer-by-layer processed ternary organic photovoltaics with efficiency over 18%. *Adv. Mater.* **2021**, *33*, 2007231. [\[CrossRef\]](#)
100. Zhang, S.; Ma, X.; Xu, C.; Xu, W.; Jeong, S.Y.; Woo, H.Y.; Zhou, Z.; Zhang, X.; Zhang, F. Boosted efficiency over 18.1% of polymer solar cells by employing large extinction coefficients material as the third component. *Macromol. Rapid Commun.* **2022**, *43*, 2200345. [\[CrossRef\]](#)
101. Guan, M.; Tao, W.; Xu, L.; Qin, Y.; Zhang, J.; Tan, S.; Huang, M.; Zhao, B. An asymmetric small-molecule donor enables over 18% efficiency in ternary organic solar cells. *J. Mater. Chem. A* **2022**, *10*, 9746–9752. [\[CrossRef\]](#)
102. Jin, K.; Ou, Z.; Zhang, L.; Yuan, Y.; Xiao, Z.; Song, Q.; Yi, C.; Ding, L. A chlorinated lactone polymer donor featuring high performance and low cost. *J. Semicond.* **2022**, *43*, 050501. [\[CrossRef\]](#)
103. Bai, H.R.; An, Q.; Jiang, M.; Ryu, H.S.; Yang, J.; Zhou, X.J.; Zhi, H.F.; Yang, C.; Li, X.; Woo, H.Y. Isogenous Asymmetric-Symmetric Acceptors Enable Efficient Ternary Organic Solar Cells with Thin and 300 nm Thick Active Layers Simultaneously. *Adv. Funct. Mater.* **2022**, *32*, 2200807. [\[CrossRef\]](#)
104. Yue, Y.; Zheng, B.; Liu, M.; Chen, Y.; Huo, L.; Wang, J.; Jiang, L. Furan-based liquid-crystalline small-molecule donor guest improving the photovoltaic performance of organic solar cells with amorphous packing. *Sci. China Mater.* **2022**, *65*, 3402–3410. [\[CrossRef\]](#)
105. Zeng, Y.; Li, D.; Wu, H.; Chen, Z.; Leng, S.; Hao, T.; Xiong, S.; Xue, Q.; Ma, Z.; Zhu, H. Enhanced Charge Transport and Broad Absorption Enabling Record 18.13% Efficiency of PM6: Y6 Based Ternary Organic Photovoltaics with a High Fill Factor Over 80%. *Adv. Funct. Mater.* **2022**, *32*, 2110743. [\[CrossRef\]](#)
106. Lan, A.; Lv, Y.; Zhu, J.; Lu, H.; Do, H.; Chen, Z.-K.; Zhou, J.; Wang, H.; Chen, F.; Zhou, E. High-Performance Ternary Organic Solar Cells through Incorporation of a Series of A2-A1-D-A1-A2 Type Nonfullerene Acceptors with Different Terminal Groups. *ACS Energy Lett.* **2022**, *7*, 2845–2855. [\[CrossRef\]](#)
107. Zuo, L.; Jo, S.B.; Li, Y.; Meng, Y.; Stoddard, R.J.; Liu, Y.; Lin, F.; Shi, X.; Liu, F.; Hillhouse, H.W. Dilution effect for highly efficient multiple-component organic solar cells. *Nat. Nanotechnol.* **2022**, *17*, 53–60. [\[CrossRef\]](#)
108. Li, Y.; Cai, Y.; Xie, Y.; Song, J.; Wu, H.; Tang, Z.; Zhang, J.; Huang, F.; Sun, Y. A facile strategy for third-component selection in non-fullerene acceptor-based ternary organic solar cells. *Energy Environ. Sci.* **2021**, *14*, 5009–5016. [\[CrossRef\]](#)
109. Yan, Y.; Zhang, Y.; Liu, Y.; Shi, Y.; Qiu, D.; Deng, D.; Zhang, J.; Wang, B.; Adil, M.A.; Amin, K. Simultaneously Decreasing the Bandgap and Voc Loss in Efficient Ternary Organic Solar Cells. *Adv. Energy Mater.* **2022**, *12*, 2200129. [\[CrossRef\]](#)
110. Wang, D.; Zhou, G.; Li, Y.; Yan, K.; Zhan, L.; Zhu, H.; Lu, X.; Chen, H.; Li, C.Z. High-Performance Organic Solar Cells from Non-Halogenated Solvents. *Adv. Funct. Mater.* **2022**, *32*, 2107827. [\[CrossRef\]](#)
111. Zhang, T.; An, C.; Bi, P.; Lv, Q.; Qin, J.; Hong, L.; Cui, Y.; Zhang, S.; Hou, J. A thiadiazole-based conjugated polymer with ultradeep homo level and strong electroluminescence enables 18.6% efficiency in organic solar cell. *Adv. Energy Mater.* **2021**, *11*, 2101705. [\[CrossRef\]](#)
112. Lu, H.; Li, D.; Ran, G.; Chen, Y.-N.; Liu, W.; Wang, H.; Li, S.; Wang, X.; Zhang, W.; Liu, Y. Designing High-Performance Wide Bandgap Polymer Donors by the Synergistic Effect of Introducing Carboxylate and Fluoro Substituents. *ACS Energy Lett.* **2022**, *7*, 3927–3935. [\[CrossRef\]](#)
113. Cai, Y.; Li, Y.; Wang, R.; Wu, H.; Chen, Z.; Zhang, J.; Ma, Z.; Hao, X.; Zhao, Y.; Zhang, C. A well-mixed phase formed by two compatible non-fullerene acceptors enables ternary organic solar cells with efficiency over 18.6%. *Adv. Mater.* **2021**, *33*, 2101733. [\[CrossRef\]](#)
114. Li, Y.; Guo, Y.; Chen, Z.; Zhan, L.; He, C.; Bi, Z.; Yao, N.; Li, S.; Zhou, G.; Yi, Y. Mechanism study on organic ternary photovoltaics with 18.3% certified efficiency: From molecule to device. *Energy Environ. Sci.* **2022**, *15*, 855–865. [\[CrossRef\]](#)
115. Jin, K.; Xiao, Z.; Ding, L. 18.69% PCE from organic solar cells. *J. Semicond.* **2021**, *42*, 060502. [\[CrossRef\]](#)
116. Duan, X.; Song, W.; Qiao, J.; Li, X.; Cai, Y.; Wu, H.; Zhang, J.; Hao, X.; Tang, Z.; Ge, Z. Ternary strategy enabling high-efficiency rigid and flexible organic solar cells with reduced non-radiative voltage loss. *Energy Environ. Sci.* **2022**, *15*, 1563–1572. [\[CrossRef\]](#)
117. Wang, J.; Zhang, M.; Lin, J.; Zheng, Z.; Zhu, L.; Bi, P.; Liang, H.; Guo, X.; Wu, J.; Wang, Y. An asymmetric wide-bandgap acceptor simultaneously enabling highly efficient single-junction and tandem organic solar cells. *Energy Environ. Sci.* **2022**, *15*, 1585–1593. [\[CrossRef\]](#)
118. Bi, P.; Zhang, S.; Chen, Z.; Xu, Y.; Cui, Y.; Zhang, T.; Ren, J.; Qin, J.; Hong, L.; Hao, X. Reduced non-radiative charge recombination enables organic photovoltaic cell approaching 19% efficiency. *Joule* **2021**, *5*, 2408–2419. [\[CrossRef\]](#)
119. He, C.; Pan, Y.; Ouyang, Y.; Shen, Q.; Gao, Y.; Yan, K.; Fang, J.; Chen, Y.; Ma, C.-Q.; Min, J. Manipulating the D: A interfacial energetics and intermolecular packing for 19.2% efficiency organic photovoltaics. *Energy Environ. Sci.* **2022**, *15*, 2537–2544. [\[CrossRef\]](#)
120. Sun, R.; Wu, Y.; Yang, X.; Gao, Y.; Chen, Z.; Li, K.; Qiao, J.; Wang, T.; Guo, J.; Liu, C. Single-junction organic solar cells with 19.17% efficiency enabled by introducing one asymmetric guest acceptor. *Adv. Mater.* **2022**, *34*, 2110147. [\[CrossRef\]](#)

121. Zhan, L.; Li, S.; Li, Y.; Sun, R.; Min, J.; Chen, Y.; Fang, J.; Ma, C.Q.; Zhou, G.; Zhu, H. Manipulating charge transfer and transport via intermediary electron acceptor channels enables 19.3% efficiency organic photovoltaics. *Adv. Energy Mater.* **2022**, *12*, 2201076. [\[CrossRef\]](#)
122. Zhu, L.; Zhang, M.; Xu, J.; Li, C.; Yan, J.; Zhou, G.; Zhong, W.; Hao, T.; Song, J.; Xue, X. Single-junction organic solar cells with over 19% efficiency enabled by a refined double-fibril network morphology. *Nat. Mater.* **2022**, *21*, 656–663. [\[CrossRef\]](#)
123. Lang, K.; Guo, Q.; He, Z.; Bai, Y.; Yao, J.; Wakeel, M.; Alhodaly, M.S.; Hayat, T.; Tan, Z. High performance tandem solar cells with inorganic perovskite and organic conjugated molecules to realize complementary absorption. *J. Phys. Chem. Lett.* **2020**, *11*, 9596–9604. [\[CrossRef\]](#)
124. Zhan, L.; Li, S.; Li, Y.; Sun, R.; Min, J.; Bi, Z.; Ma, W.; Chen, Z.; Zhou, G.; Zhu, H. Desired open-circuit voltage increase enables efficiencies approaching 19% in symmetric-asymmetric molecule ternary organic photovoltaics. *Joule* **2022**, *6*, 662–675. [\[CrossRef\]](#)
125. Gong, Y.; Yu, R.; Gao, H.; Ma, Z.; Dong, Y.; Su, Y.-J.; Chen, T.-W.; Hsu, C.-S.; Tan, Z. Improving charge transport and reducing non-radiative energy loss via a nonacyclic carbazole-based third component for over 18% efficiency polymer solar cells. *J. Mater. Chem. A* **2022**, *10*, 7090–7098. [\[CrossRef\]](#)

**Disclaimer/Publisher's Note:** The statements, opinions and data contained in all publications are solely those of the individual author(s) and contributor(s) and not of MDPI and/or the editor(s). MDPI and/or the editor(s) disclaim responsibility for any injury to people or property resulting from any ideas, methods, instructions or products referred to in the content.